

FOSSIL IMPRINT OF A POWERFUL FLARE AT THE GALACTIC CENTRE ALONG THE MAGELLANIC STREAM

J. BLAND-HAWTHORN¹

Sydney Institute for Astronomy, School of Physics A28, University of Sydney, NSW 2006, Australia

PHILIP R. MALONEY

CASA, University of Colorado, Boulder, CO 80309-0389, USA

RALPH S. SUTHERLAND

Mount Stromlo Observatory, Australia National University, Woden, ACT 2611, Australia

G. J. MADSEN

Institute of Astronomy, University of Cambridge, Madingley Rd, Cambridge, CB3 0HA, UK

Draft version November 5, 2018

ABSTRACT

The *Fermi* satellite discovery of the gamma-ray emitting bubbles extending 50° (10 kpc) from the Galactic Centre has revitalized earlier claims that our Galaxy has undergone an explosive episode in the recent past. We now explore a new constraint on such activity. The Magellanic Stream is a clumpy gaseous structure free of stars trailing behind the Magellanic Clouds, passing over the South Galactic Pole (SGP) at a distance of at least 50–100 kpc from the Galactic Centre. Several groups have detected faint $H\alpha$ emission along the Magellanic Stream ($1.1 \pm 0.3 \times 10^{-18}$ erg cm⁻² s⁻¹ arcsec⁻²) that is a factor of 5 too bright to have been produced by the Galactic stellar population. The brightest emission is confined to a cone with half angle $\theta_{1/2} \approx 25^\circ$ roughly centred on the SGP. Time-dependent models of Stream clouds exposed to a flare in ionising photon flux show that the ionised gas must recombine and cool for a time interval $T_o = 0.6$ – 2.9 Myr for the emitted $H\alpha$ surface brightness to drop to the observed level. A nuclear starburst is ruled out by the low star formation rates across the inner Galaxy, and the non-existence of starburst ionisation cones in external galaxies extending more than a few kiloparsecs. Sgr A^{*} is a more likely candidate because it is two orders of magnitude more efficient at converting gas to UV radiation. The central black hole ($M_\bullet \approx 4 \times 10^6 M_\odot$) can supply the required ionising luminosity with a fraction of the Eddington accretion rate ($f_E \sim 0.03$ – 0.3 , depending on uncertain factors, e.g., Stream distance), typical of Seyfert galaxies. In support of nuclear activity, the $H\alpha$ emission along the Stream has a polar angle dependence peaking close to the SGP. Moreover, it is now generally accepted that the Stream over the SGP must be further than the Magellanic Clouds. At the lower halo gas densities, shocks become too ineffective and are unlikely to give rise to a polar angle dependence in the $H\alpha$ emission. Thus it is plausible that the Stream $H\alpha$ emission arose from a ‘Seyfert flare’ that was active 1–3 Myr ago, consistent with the cosmic ray lifetime in the *Fermi* bubbles. Such a flare may have been causally linked to one of the episodes of massive star formation triggered in close proximity to Sgr A^{*} within the last few Myr. Sgr A^{*} activity today is greatly suppressed (70–80 dB) relative to the Seyfert outburst. The rapid change over a huge dynamic range in ionising luminosity argues for a compact UV source with an extremely efficient (presumably magneto-hydrodynamic) ‘drip line’ onto the accretion disk.

1. INTRODUCTION

Nuclear activity powered by a supermassive black hole is a remarkable phenomenon that allows galaxies to be observed to at least a redshift $z \approx 7$ (e.g. Mortlock et al 2011). Evidence is beginning to emerge that our Galaxy has experienced possibly related episodes in the recent past. The proximity of the Galactic Centre provides us with an opportunity to study this activity in unprecedented detail.

The first evidence for a large-scale bipolar outflow came from extended bipolar *ROSAT* 1.5 keV X-ray and *MSX* 8.3 μ m mid-infrared emission observed to be associated with the Galactic Centre (Bland-Hawthorn & Cohen 2003). Two observations made clear that this activity *must* be associated with

the centre of the Galaxy: (i) the bipolar structure is not visible in the diffuse *ROSAT* 0.2–0.5 keV data because the disk is optically thick at these energies; (ii) a hard X-ray bipolar counterpart has never been observed from a blow-out due to a young star cluster, thereby ruling out any association with a spiral arm along the line of sight. Further support for the large-scale wind picture comes from a population of entrained $H\text{I}$ clouds (McClure-Griffiths et al 2013) and from the kinematics of low-column halo clouds observed in absorption along quasar sight lines (Keeney et al 2006). In summary, the wind energetics are estimated to be roughly 10^{55} erg visible over 20° (5 kpc in radius).

In 2010, spectacular evidence for a powerful nuclear event came from *Fermi* gamma-ray satellite observations (1–100 GeV) of giant bipolar bubbles extending 50° (10 kpc) from the Galactic Centre (Su et al 2010). The source of the bubbles,

¹ Visiting Fellow, Australian Astronomical Observatory, 105 Delhi Rd, North Ryde, NSW 2113, Australia

whether related to starburst or AGN activity, remains hotly contested (Zubovas et al 2011; Su & Finkbeiner 2012; Carretti et al 2013). The bubbles appear to be associated with the very extended radio emission (‘haze’) first identified in *WMAP* microwave observations (Finkbeiner 2004) and are clearly associated with the bipolar X-ray structures (Bland-Hawthorn & Cohen 2003). One interpretation is that the gamma-ray photons arise through inverse Compton scattering of the interstellar and cosmic background radiation field by high energy cosmic rays (10–100 GeV) from the black hole accretion disk (Su et al 2010; Dobler et al 2010). In this scenario, the cosmic ray cooling times T_{CR} are of order a few million years, suggesting powerful nuclear activity on a similar timescale. This picture implicates very fast nuclear winds with speeds of order ~ 10 kpc/ $T_{CR} \sim 10^4$ km s $^{-1}$.

Guo & Mathews (2012) have recently challenged the wind picture on the grounds that the diffusion coefficient for cosmic rays advected in winds is much lower than required to explain the Fermi bubbles. Instead, they suggest the cosmic rays are carried by bipolar jets from an active galactic nucleus (AGN) which inflated the Fermi bubbles. Spectacular examples of this phenomenon do exist in nearby Seyfert galaxies (e.g. 0313-192; Keel et al 2006). Preliminary evidence for nuclear jets at the Galactic Centre has been discussed by several authors (Su & Finkbeiner 2012; Yusef-Zadeh et al 2012). In the Guo & Mathews model, the jets formed 1–3 Myr ago and endured for 0.1–0.5 Myr with a total energy in the range 10^{55-57} erg.

The supermassive black hole associated with the Galactic Centre source Sgr A* has a well established mass¹ with 10% uncertainty ($M_{\bullet} \approx 4 \times 10^6 M_{\odot}$; Genzel et al 2003; Meyer et al 2012). At the present time, little is known about past nuclear activity. It is likely that the black hole was far more active before a redshift of unity when galactic accretion was at its peak. But even at the present epoch, there is good evidence for enhanced nuclear activity in interacting L^* galaxies (q.v. Wild et al 2013; Rupke & Veilleux 2013). Direct evidence that the nuclear regions were much brighter in the past comes from ASCA 2–10 keV observations of circumnuclear clouds (Sunyaev et al 1993; Koyama et al 1996) with indications that Sgr A* was 10^5 times more active within the past 10^3 years (q.v. Ponti et al 2010). More compelling evidence on much longer timescales comes from the existence of the Fermi bubbles.

We now show that if our Galaxy went through a Seyfert phase in the recent past, it could conceivably have been so UV bright that it lit up the Magellanic Stream over the South Galactic Pole (SGP) through photoionisation. Interestingly, the Magellanic Stream has detectable $H\alpha$ emission along its length that is at least 5 times more luminous than can be explained by UV escaping from the Galaxy (see §2). Ionisation cones have been observed in several dozen Seyfert galaxies to date. Arguably, the most spectacular example is the S0 galaxy NGC 5252 (Tadhunter & Tsvetanov 1989): orbiting gas streams up to 30 kpc in radius are lit up along bipolar cones due to the nuclear UV flux (Tsvetanov et al 1996). Kreimeyer & Veilleux (2013) have discovered ionisation cones in MR2251-178, a nearby quasar with a weak double-lobed radio source; non-thermal photoionisation is seen out to 90 kpc in radius emphasising the extraordinary reach of AGN activity to the present day.

In principle, the Stream $H\alpha$ emission could have been pro-

duced by a starburst event in the Galactic Centre, rather than by a Seyfert flare. However, as we discuss in Appendix B, the required star formation rate of such a starburst is at least two orders of magnitude larger than allowed by the star formation history of the Galactic Centre. An accretion flare from Sgr A* is a much more probable candidate for the ionisation source because (a) an accretion disk converts gas to ionising radiation with much greater efficiency than star formation, thus minimizing the fuelling requirements; (b) there is an abundance of material in the vicinity of Sgr A* to fuel such an outburst, and (c) a rapid decline in the ionising luminosity, needed in both starburst and AGN models to reconcile the present-day lack of activity with the magnitude of the required flare, is prohibitively difficult for starburst models but achievable (and interestingly challenging) for accretion disk models (cf. §5.1). Regardless of the true origin of the Stream’s $H\alpha$ emission, we show that its brightness is a powerful constraint on recent nuclear activity.

In §2, we describe basic properties of the Magellanic Stream and derive the levels of ionisation required to explain the observations. In §3, we carry out time dependent ionisation calculations and relate to past AGN activity. We suggest follow-up observations in §4 and discuss the implications of our findings in §5. We conclude the paper with extended supplementary material on the gas physics, ionisation requirements and the ionisation spectrum in three appendices.

2. EXPERIMENT

Target. The Magellanic Stream (Fig. 1a) lies along a great arc that extends for more than 150° (Mathewson, Cleary & Murray 1974; Putman et al 1998; Nidever et al 2008). Fig. 1b illustrates the relationship of the LMC to the Magellanic Stream above the Galactic disk along a circular orbit originating from the Lagrangian point between the LMC and the SMC, at a Galactocentric distance of 55 kpc (Mathewson & Ford 1984). More recent simulations tend to suggest that the LMC-SMC system is infalling for the first time with an orbital period of order a Hubble time (Besla et al 2012; Nichols et al 2011). This implies substantial ellipticity of the orbit with the Stream distance over the SGP falling within the range 80–150 kpc (Model 1; Besla et al 2012). Given the uncertain mass of the Galactic halo (Kafle et al 2012), the drag coefficient of the Stream gas, and the initial orbit parameters of the Magellanic Clouds, the true distance along the SGP is unlikely to exceed 100 kpc (Jin & Lynden-Bell 2008).

The Magellanic Stream is made up of a series of dense gas clumps with column densities that vary over at least a factor of ten (Moore & Davis 1994; Putman et al 1998). Even the diffuse gas between the dense clouds is optically thick to the Lyman continuum ($> 1.6 \times 10^{17}$ cm $^{-2}$). In the clouds, a mean column density of $N_c \sim 7 \times 10^{19}$ cm $^{-2}$ and a mean cloud size of $d_c \sim 1$ kpc leads to a total hydrogen density spanning the range $n_H \approx 0.03$ – 0.2 cm $^{-3}$. This leads to a typical spherical cloud mass of roughly $M_c \sim m_p N_c d_c^2 / 2 \sim 10^6 M_{\odot}$, for which m_p is the proton mass. In reality, the gas may have a fractal distribution in density (Bland-Hawthorn et al 2007; Stanimirovic et al 2008; Nigra et al 2012). The mean metallicity of the Magellanic Stream appears to be everywhere one tenth of the solar value (Fox et al 2013) although isolated regions close to the Magellanic Clouds are more enriched (Richter et al 2013).

H α observations. Weiner & Williams (1996) made the remarkable discovery of relatively bright $H\alpha$ emission along the

¹ For a review of all estimates of M_{\bullet} to date, see Kormendy & Ho (2013).

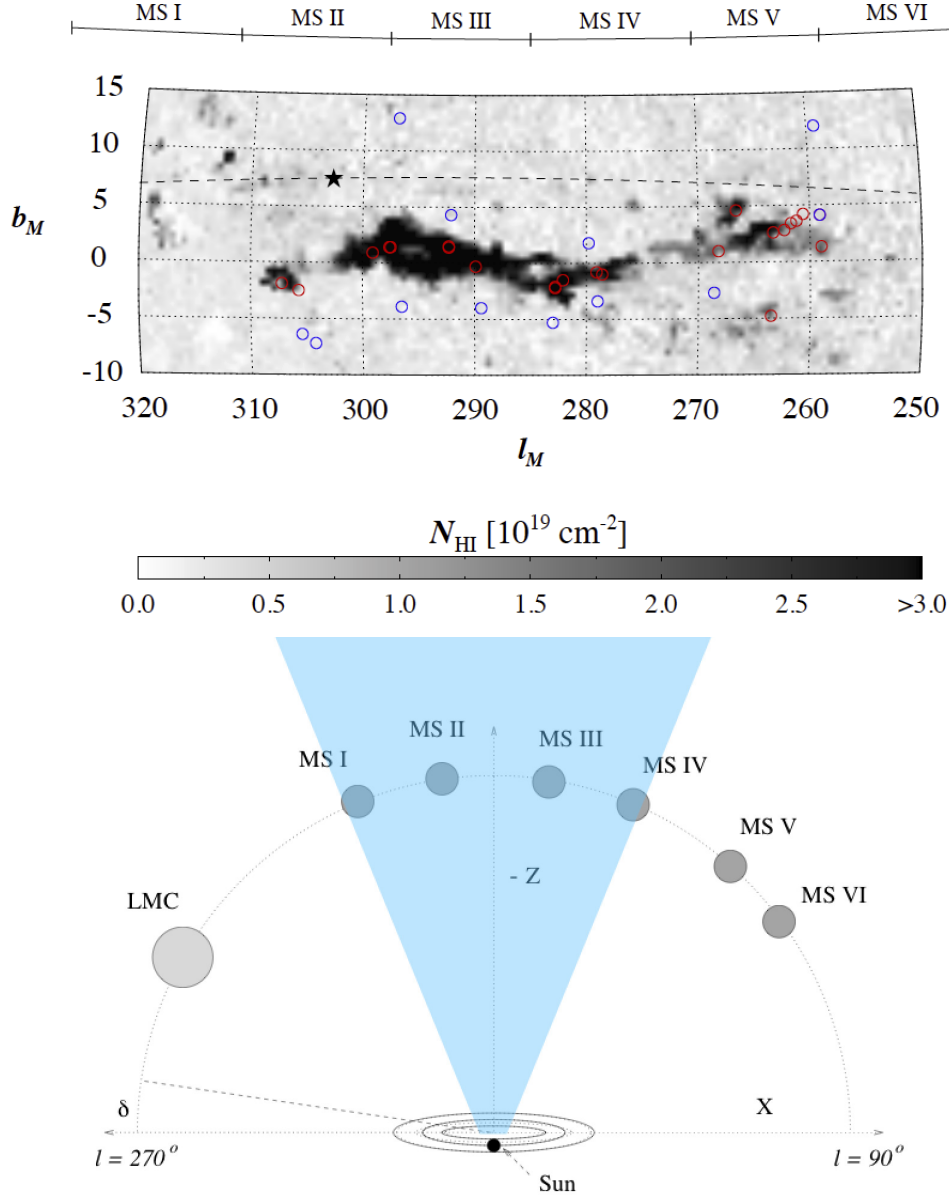


FIG. 1.— (Top) HI column density map of the Magellanic Stream (adapted from Madsen 2012). The coordinates are in Magellanic longitude and latitude (ℓ_M, b_M), as defined by Nidever et al (2008), and the asterisk indicates the SGP. The linear greyscale shows the column density of HI from the LAB survey (Kalberla et al. 2005), with the 21cm emission integrated over the velocity range of $-450 \text{ km s}^{-1} < v_{\text{LSR}} < -100 \text{ km s}^{-1}$. The location and 1° field of view of the new WHAM observations are shown as red and blue circles, corresponding to target and sky observations, respectively. The approximate longitudinal extents of the six Stream complexes (identified by Mathewson & Ford 1984) are shown on the top of the figure. (Bottom) An illustration of the LMC and the dominant clouds in the Magellanic Stream (Mathewson & Ford 1984) projected onto the Galactic X-Z plane. The orbit of the Stream lies close to the great circle whose Galactic longitude is $\ell = 280^\circ$ (lhs of SGP) and $\ell = 100^\circ$ (rhs of SGP) shown as a dashed line. The blue fan illustrates the proposed ionisation cone from the Galactic Centre.

Magellanic Stream when compared to high-velocity clouds (HVC) close to the Galactic plane. These detections have been confirmed and extended through follow-up observations (Weiner et al 2002; Putman et al 2003; Madsen 2012) that are summarised in Fig. 2. The figure shows the $\text{H}\alpha$ surface brightness observations along the Stream as a function of Magellanic longitude ℓ_M , where ℓ_M is defined in a plane that lies close to a great circle passing through the South Galactic Pole (Nidever 2008). Solid symbols show detections; open symbols show non-detections. In order to minimize the effects of bright, time-variable atmospheric emission lines, the

data taken with the Wisconsin H-Alpha Mapper (WHAM) employed an offset sky subtraction technique (Madsen et al 2001). The high spectral resolution of the WHAM data enables us to confirm the association of the ionised gas with the cold Stream gas; the H I and $\text{H}\alpha$ velocities are consistent with each other to within $\approx 5 \text{ km s}^{-1}$. The densities and length scales for the H I clouds derived above are within range of the expected values to account for the mean $\text{H}\alpha$ surface brightness. Furthermore, the beam size for most of the $\text{H}\alpha$ measurements (1° for WHAM) is of order the mean projected cloud size and thus provides an average estimate for the cloud.

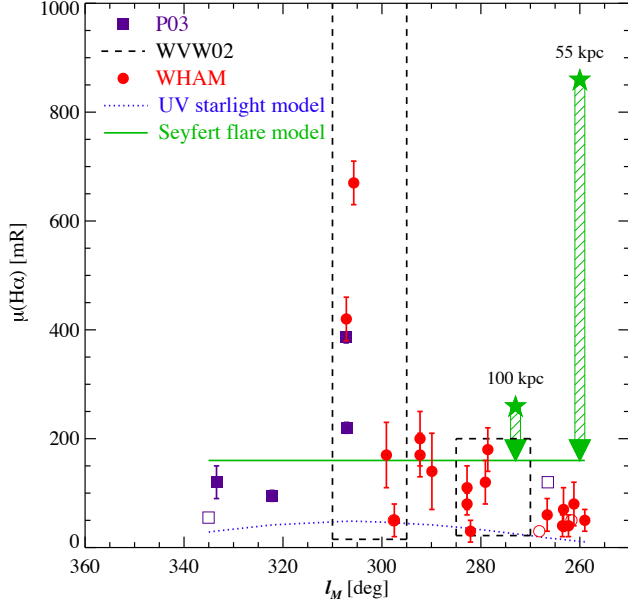


FIG. 2.— Observations and models of $H\alpha$ emission along the Magellanic Stream. The dashed boxes indicate the range of detected values from Weiner et al (2002); the purple points are from Putman et al (2003); the red points are new observations from WHAM (Madsen 2012). The extreme $H\alpha$ values occur close to the SGP at $\ell_M \approx 303^\circ$. The dotted blue curve is the upper bound of allowed UV ionisation from the Galaxy (disk+bulge+hot gas) from the model of Bland-Hawthorn & Maloney (1999). The green arrows illustrate the effect of a fading Seyfert flare ($f_E = 0.1$) for Stream distances of 55 kpc (long arrow) and 100 kpc (short arrow). The horizontal green line indicates a characteristic $H\alpha$ surface brightness (160 mR).

However, the origin of this emission remains highly uncertain.

Stream ionisation. We adopt physically motivated units that relate the ionising photon flux at a distant cloud to the resultant $H\alpha$ emission. For this, we need to relate the plasma column emission rate to a photon surface brightness. In keeping with astronomical research on diffuse emission (e.g. WHAM survey – Reynolds et al 1998), we use the Rayleigh unit introduced by aeronomers (q.v. Baker & Romick 1976) which is a unique measure of *photon* intensity; 1 milliRayleigh (mR) is equivalent to $10^3/4\pi$ photons $\text{cm}^{-2} \text{s}^{-1} \text{sr}^{-1}$. The emission measure \mathcal{E}_m for a plasma with electron density n_e is given by (e.g. Spitzer 1978)

$$\mathcal{E}_m = \int f_i n_e^2 dz \quad \text{cm}^{-6} \text{pc} \quad (1)$$

which is an integral of H recombinations along the line of sight z multiplied by a filling factor f_i . The suffix i indicates that we are referring to the volume over which the gas is ionised. For a plasma at 10^4K , $\mathcal{E}_m(H\alpha) = 1 \text{ cm}^{-6} \text{pc}$ is equivalent to an $H\alpha$ surface brightness of 330 milliRayleighs (mR). In cgs units, this is equivalent to $1.9 \times 10^{-18} \text{ erg cm}^{-2} \text{s}^{-1} \text{arcsec}^{-2}$ which would be a faint spectral feature in a 1 hr integration using a slit spectrograph on an 8m telescope. But for the Fabry-Perot ‘staring’ technique employed in Fig. 2, this is an easy detection if the diffuse emission uniformly fills the aperture. We refer to the Stream $H\alpha$ emission as relatively bright because it is much brighter than expected for an optically thick cloud at a distance of 50 kpc or more from the Galactic Centre.

The characteristic $H\alpha$ surface brightness observed along the Stream of $\mu_{H\alpha} \approx 160 \text{ mR}$ (Fig. 2) can be used to set a

minimum required ionising photon flux and luminosity for a Galactic Centre flare, assuming that the Stream emission has not begun to fade and that there is no absorption or extinction of the ionising photon flux prior to reaching the Stream. For a slab ionized on one side, this is

$$\varphi_{i,\min} \approx 3.9 \times 10^5 \text{ phot cm}^{-2} \text{s}^{-1} \quad (2)$$

The implied ionising photon luminosities are then

$$N_{i,\min} \approx (1.4 - 4.7) \times 10^{53} \text{ phot s}^{-1} \quad (3)$$

for $D = 55 - 100 \text{ kpc}$. Any model in which the Stream emission is produced by a nuclear outburst must explain the magnitude of this ionising photon luminosity.

Expected emission via the Galactic stellar population. First we consider the expected emission due to the ionizing radiation from the Galactic stellar population and associated sources. The total flux at a frequency ν reaching an observer located at a distance D is obtained from integrating the specific intensity I_ν over the surface of a disk, i.e.

$$F_\nu = \int_A I_\nu(\mathbf{n})(\mathbf{n} \cdot \mathbf{N}) \frac{dA}{D^2} \quad (4)$$

where \mathbf{n} and \mathbf{N} are the directions of the line of sight and the outward normal to the surface of the disk, respectively. At this stage, we consider only an isotropic illumination source rather than more complex forms of illumination with a strong polar angle dependence. In this instance, we use the more familiar scalar form of eq. (4) such that

$$\varphi_* = \int_\nu \frac{F_\nu}{h\nu} \cos \theta d\nu \quad (5)$$

where φ_* is the photoionising flux from the stellar population, $\mathbf{n} \cdot \mathbf{N} = \cos \theta$ and h is Planck’s constant. This is integrated over frequency from the Lyman limit ($\nu = 13.6 \text{ eV}/h$) to infinity to convert to units of photon flux ($\text{phot cm}^{-2} \text{s}^{-1}$). The photon spectrum of the Galaxy is a complex time-averaged function of energy N_* (photon rate per unit energy) such that $4\pi D^2 \varphi_* = \int_0^\infty N_*(E) dE$.

For a given ionising luminosity, we can determine the expected $H\alpha$ surface brightness at the distance of the Magellanic Stream. For an optically thick cloud ionised on one side, we relate the emission measure to the ionising photon flux using $\mathcal{E}_m = 1.25 \times 10^{-6} \varphi_* \text{ cm}^{-6} \text{pc}$ (Bland-Hawthorn & Maloney 1999). The total ionising luminosity of the Galaxy is now well established within a small factor (Bland-Hawthorn & Maloney 1999; Weiner et al 2002; Putman et al 2003). For a total disk star formation rate of $1.1 \pm 0.4 \text{ M}_\odot \text{yr}^{-1}$ (Robitaille & Whitney 2010), the hot young stars produce an integrated photon flux over the disk of $2.6 \times 10^{53} \text{ phot s}^{-1}$ with very few photons beyond 50 eV.

The mean vertical opacity of the disk at the Lyman limit is $\tau_{LL} = 2.8 \pm 0.4$, equivalent to a vertical escape fraction of $f_{*,\text{esc}} \approx 6\%$ perpendicular to the disk ($\mathbf{n} \cdot \mathbf{N} = 1$). The Galactic UV contribution at the distance D of the Magellanic Stream is given by

$$\mu_{*,H\alpha} = 21 \zeta \left(\frac{f_{*,\text{esc}}}{0.06} \right) \left(\frac{D}{55 \text{ kpc}} \right)^{-2} \text{ mR}. \quad (6)$$

corresponding to $\varphi_i \approx 5.1 \times 10^4 \text{ phot s}^{-1}$. The correction factor $\zeta \approx 2$ is included to accommodate weakly constrained ionising contributions from the old stellar population, hot gas

(disk+halo) and the Magellanic Clouds (Slavin et al 2000; Bland-Hawthorn & Maloney 2002; Barger et al 2013). We arrive at the blue curve presented in Fig. 2 which fails to explain the observed $H\alpha$ emission by at least a factor of 5.

We note that if the Stream is more distant at 100 kpc, preferred by some recent models (Besla et al 2012), the predicted emission measure due to the Galaxy approaches the upper limit (~ 8 mR at 2σ) obtained by Weymann et al (2001). The discrepancy with the observed $H\alpha$ brightness is now a factor of 20!

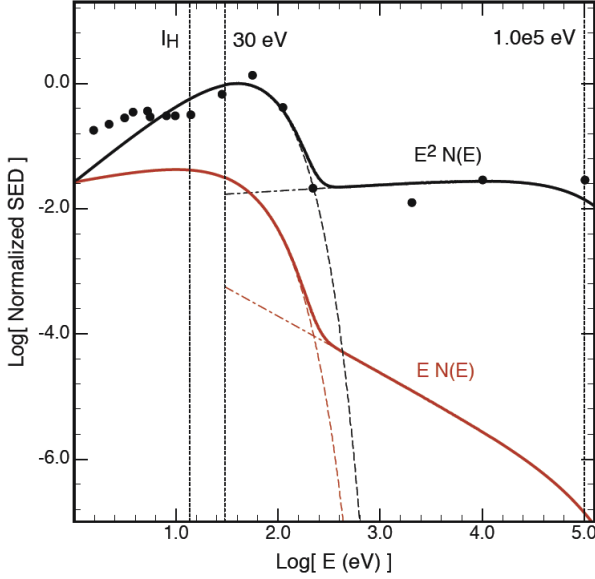


FIG. 3.— The energy spectrum of the Galactic Centre accretion disk (see Appendix C) is assumed to comprise a ‘big blue bump’ and an X-ray + γ -ray power law component. The lower curve is the photon spectrum $E N_\bullet(E)$. The upper curve is the energy-weighted photon spectrum $E^2 N_\bullet(E)$ which serves to illustrate that there is an order of magnitude more energy in the big blue bump ($\eta = 9$) than the hard energy tail. The data points are taken from the nuclear ionising spectrum derived from the *ISO-SWS* (2–200 μ m) satellite data for NGC 1068.

Nuclear spectrum. We now consider the Stream emission due to ionizing radiation powered by the supermassive black hole at the Galactic Centre. Motivated by detailed spectral observations of AGN, we adopt a two-component accretion-disk model for the photon spectrum of the central source. We define the specific photon luminosity for the two-component model by

$$N_\bullet = k_1 (E/E_1)^{-2/3} e^{-E/E_1} + k_2 (E/E_2)^{-\alpha} e^{-E/E_2} \mathcal{H}(E - E_1) \quad \text{phot s}^{-1} \text{ eV}^{-1} \quad (7)$$

where $\mathcal{H}[E - E_1] = 1$ if $E > E_1$ and $\mathcal{H}[E - E_1] = 0$ otherwise. The first term on the rhs of eq. (7) represents the cool, optically thin Shakura-Sunyaev spectrum thought to produce the enhanced UV (“big blue bump”) emission observed in Seyfert galaxies and quasars (Antonucci 1993). The second term represents the X-ray and gamma-ray emission observed from the source. We choose $E_1 = 30$ eV for the cool outer blackbody spectrum, $\alpha = 1.9$ for the photon spectral index of the X- γ component (i.e., 0.9 for the energy spectral index), and adopt $E_2 = 100$ keV (Dermer et al 1997).

By integrating eq. (7) weighted by energy, we derive the relative normalisation constants k_1 and k_2 (see Appendix C).

The ionising spectrum of NGC 1068 is strongly constrained by 2–200 μ m *ISO-SWS* observations (Alexander et al 2000; Lutz et al 2000). This barred spiral galaxy has the most extensive literature of any Seyfert and serves as a surrogate for the AGN activity at the Galactic Centre. We have used the unattenuated spectrum to normalize our composite model. We find that $\eta \approx 9$ ($\log k_1/k_2 = 8.8663$) provides a reasonable match to NGC 1068. Our assumed ionising spectrum of the Galaxy’s AGN presented in Fig. 3 has the same functional form.

The ionising flux φ_\bullet follows from eq. (7) such that $4\pi D^2 \varphi_\bullet = \int_{I_H}^\infty N_\bullet dE$ where $I_H = 13.598$ eV. The spectrum is dominated by the soft component such that estimates of the AGN-induced $H\alpha$ emission (below) are not obfuscated by the longer mean free paths of the harder photons. Thus properties derived from the stellar (φ_\star) and AGN (φ_\bullet) photon fluxes can be compared directly; the photons propagate roughly the same depth into an $H\text{I}$ cloud.

Expected emission from an active nucleus. We now relate the accretion disk luminosity L_\bullet to the properties of the supermassive black hole. An accreting black hole converts rest-mass energy with a conservative efficiency $\epsilon = 5\%$ into radiation with a luminosity ($= \epsilon \dot{m} c^2$)

$$L_\bullet \approx 7.3 \times 10^{11} \left(\frac{\epsilon}{0.05} \right) \left(\frac{\dot{m}}{M_\odot \text{ yr}^{-1}} \right) L_\odot \quad (8)$$

for which \dot{m} is the mass accretion rate. The accretion disk luminosity can limit the accretion rate through radiation pressure. The so-called Eddington limit is given by

$$L_E = \frac{4\pi G M_\bullet m_p c}{\sigma_T} \quad (9)$$

$$= 1.4 \times 10^{11} \left(\frac{M_\bullet}{4 \times 10^6 M_\odot} \right) L_\odot \quad (10)$$

where M_\bullet is the black-hole mass and σ_T is the Thomson cross-section for electron scattering.

Radiation pressure from the accretion disk at the Galactic Centre limits the maximum accretion rate to $\dot{m} \sim 0.2 M_\odot \text{ yr}^{-1}$. Some Seyferts, including NGC 1068 (Begelman & Bland-Hawthorn 1997), radiate at close to the limit. But active galactic nuclei appear to spend most of their lives operating at a fraction f_E of the Eddington limit with rare bursts arising from accretion events (Hopkins & Hernquist 2006). For clouds at a distance of 55–100 kpc along the SGP, we now show that only a fraction of the maximum accretion rate is needed to account for the $H\alpha$ emission along the Magellanic Stream. The orbital period of the Stream is of order a Hubble time so we can consider the Stream to be a stationary target relative to ionisation timescales.

The dust levels are very low in the Stream (Fox et al 2013); internal and line-of-sight extinctions are negligible. It follows from eq. (10) that the ionising photon luminosity of the Seyfert nucleus is given by

$$N_{\bullet,i} = 7.2 \times 10^{53} \left(\frac{f_E}{0.1} \right) \left(\frac{M_\bullet}{4 \times 10^6 M_\odot} \right) \text{phot s}^{-1}. \quad (11)$$

For the photon spectrum in eq. (7), we find that 20% of the energy falls below the Lyman limit and therefore does not photoionise hydrogen. If the absorbing cloud is optically thick, the ionising flux can be related directly to an $H\alpha$ surface

brightness. The ionising flux is given by

$$\varphi_{\bullet} = 2.0 \times 10^6 \left(\frac{f_E}{0.1} \right) \left(\frac{f_{\bullet, \text{esc}}}{1.0} \right) \left(\frac{D}{55 \text{ kpc}} \right)^{-2} \text{ phot cm}^{-2} \text{ s}^{-1}. \quad (12)$$

We have included a term for the UV escape fraction from the AGN accretion disk $f_{\bullet, \text{esc}}$ ($\mathbf{n} \cdot \mathbf{N} = 1$). This is likely to be of order unity to explain the integrated energy in observed ionisation cones (Sokolowski et al 1991; Mulchaey et al 1996). Some energy is lost due to Thomson scattering but this is known to be only a few percent in the best constrained sources (e.g. NGC 1068; Krolik & Begelman 1986). In principle, the high value of $f_{\bullet, \text{esc}}$ can increase $f_{\bullet, \text{esc}}$ but the stellar bulge is not expected to make more than a 10-20% contribution to the total stellar budget (Bland-Hawthorn & Maloney 2002); a possible contribution is accommodated by the factor ζ (eq. [6]).

The expected surface brightness for clouds that lie within a putative ‘ionisation cone’ from the Galactic Centre is given by

$$\mu_{\bullet, \text{H}\alpha} = 825 b \left(\frac{f_E}{0.1} \right) \left(\frac{f_{\bullet, \text{esc}}}{1.0} \right) \left(\frac{D}{55 \text{ kpc}} \right)^{-2} \text{ mR}. \quad (13)$$

Strictly speaking, this provides us with an upper limit or ‘peak brightness.’ In §3, we show that proper consideration must be given to the physical state of the gas and the time since the event occurred. The recombination emission will fade once the burst duration has passed and the gas begins to recombine and cool. For completeness, we have included a beaming factor b to accommodate more exotic models that allow for mild beaming of the UV radiation (e.g. Acosta-Pulido et al 1990). The solid angle subtended by a half-opening angle of $\theta_{1/2}$ is $\Delta\Omega = 2\pi(1 - \cos\theta_{1/2})$. So the beam factor $b = (1 - \cos\theta_{1/2})^{-1}$ expresses how much of the isotropic radiation is channelled into a cone rather than 2π sr. For example, $\theta_{1/2} = 22.5^\circ$ is a beam factor $b = 13$; $\theta_{1/2} = 30^\circ$ is a beam factor $b = 7.5$; $\theta_{1/2} = 90^\circ$ is a beam factor $b = 1$ (isotropic emission) adopted for the remainder of the paper. The emission within an ionisation cone can be isotropic if the restriction is caused by an external screen, e.g. a dusty torus on scales much larger than the accretion disk.

3. PAST AGN ACTIVITY

3.1. Timescales

Consider the situation in which we observe the ionisation of the Stream due to a nuclear source. A burst of intense UV at a time T_o in the past, lasting for a period T_B , must propagate for a time $T_C \sim 0.18 (D/55 \text{ kpc}) \text{ Myr}$ to reach the Stream. For example, in the Seyfert jet model of Guo & Mathews (2012), $T_o \approx 1 - 3 \text{ Myr}$ and $T_B \approx 0.1 - 0.5 \text{ Myr}$. The ionisation front then moves through the cool gas until the UV is used up. This occurs in a time $T_I \sim 1/(\sigma_H \varphi_{\bullet})$ where σ_H is the H ionisation cross section. This follows from the fact that the speed of the ionisation front into the neutral gas is $q = \varphi_{\bullet}/n_H$ where q is the ionisation parameter² for a neutral H density n_H . For the H α emission levels associated with the Magellanic Stream, $T_I \sim 4 \times 10^3 / (\varphi_{\bullet}/10^6) \text{ yr}$; for simplicity, the extra factors from eq. (12) are not carried over. The time for the gas to reach ionisation equilibrium will be of order T_I , and is very short compared to both T_C and the likely values of T_o . The

H α emission is then proportional to $\alpha_B n_e N_e$, where n_e is the electron density, N_e is the column density of ionised gas, and α_B is the Case B recombination coefficient.

Since the level of activity in the Galactic Center today is far too low to produce the observed H α emission, the Stream emission in this picture is almost certainly fading from an earlier peak. The time T_d required for the emission to decrease from its peak value to the observed brightness depends on both the time evolution of the burst luminosity and the gas density in the Stream³. Since we observe the Stream as it was T_C years ago, the look-back time to the initial event is $T_o = T_d + 2T_C$ (assuming the burst time T_B is much less than T_o). We now revisit these approximations with detailed calculations of the ionisation state of the gas.

3.2. UV photoionisation

We use the recently completed *MAPPINGS IV* code (Dopita et al 2013) to study both isochoric and isobaric cooling at the surface of the Magellanic Stream. The source of the impinging radiation field is the accretion disk model presented in Fig. 3. The models were run by turning on the source of ionization, waiting for the gas to reach ionization/thermal equilibrium, and then by turning off the ionizing photon flux. In Figs. 4 and 5, we present our modelled trends in gas temperature (T_e), ionisation fraction (χ) and emission measure (\mathcal{E}_m) for time-dependent ionisation of the Magellanic stream. Important properties of the medium – ionised column depths, emission measures, cooling times, etc. – are included in Table 1. The sound crossing times of the warm ionised layers are too long ($\gtrsim 10 \text{ Myr}$) in the low density regime relevant to our study for isobaric conditions to prevail. Both a near ($D = 55 \text{ kpc}$) and a far ($D = 100 \text{ kpc}$) distance is considered.

The gas phase abundances are the solar values scaled to $[\text{Fe}/\text{H}] = -1$ now well established from *HST COS* measurements (Fox et al 2013; Richter et al 2013). The upper limits for [OI]630 nm from the WHAM survey indicate that the ionisation fraction in the brightest H α -emitting clouds exceeds $\chi = 50\%$ (Madsen et al 2013). For a spherical cloud, its mass is approximately $M_c \sim f_n \rho_c d_c^3 / 2$ where the subscript n denotes that the filling factor refers to the neutral cloud prior to external ionisation. For a fixed cloud mass (or equivalently, cloud column density N_c), the filling factor is inversely related to the H I gas density. Any value other than unity leads to higher gas densities, and shorter recombination times. While the cloud geometry and the volume filling factor are uncertain (Fox et al 2010), self-consistent ionisation parameters q are obtained at all times and lie within the range $\log q = 5.6 - 7.6$ ($\log u \approx -5$ to -3).

In Fig. 5, the initial photoionising flash rapidly heats the gas to a peak temperature before the gas begins recombining at a rate that is inversely proportional to n_H as expected (§2). We observe that the recombination rate is faster than the cooling rate during this period. The initial flash produces high ionisation states (e.g. He II, [O III] emission lines) but these fade rapidly. In Fig. 4, the increase in electron density leads to a maximum H α brightness which then also fades. The Balmer decrement $\text{H}\alpha/\text{H}\beta$ is everywhere in the range 3.0–3.1 until very late times when it begins to climb, except now the flare ionisation signal has almost faded from view. While the decrement is sensitive to dust extinction, the low metallicity of the Stream has negligible impact on this diagnostic (see §5).

² This is often defined as the dimensionless ionisation parameter $u = q/c$.

³ This is discussed in detail in §5.1 and Appendix A.

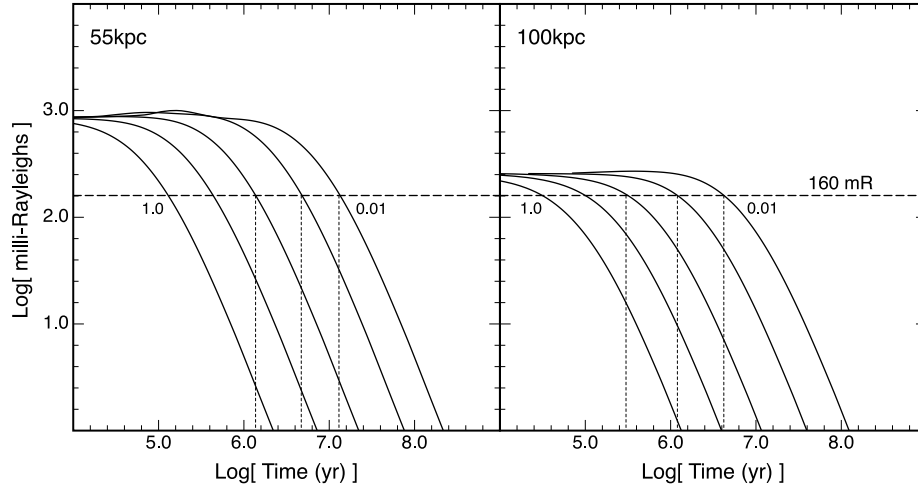


FIG. 4.— *MAPPINGS IV* time-dependent isochoric calculations of the change in $H\alpha$ surface brightness after a Seyfert flare has occurred at the Galactic Centre. (Left) $D = 55$ kpc, $f_E = 0.1$; (Right) $D = 100$ kpc, $f_E = 0.1$. From left to right, the pre-ionised gas densities are 1.0, 0.3, 0.1, 0.03, 0.01 cm^{-3} . The clouds have 0.1 Z_\odot metallicity and are irradiated by an AGN accretion disk (see text). The mean surface brightness of the Stream near the SGP (160 mR) is shown as a horizontal dashed line. Physical properties of the models are to be found in Table 1.

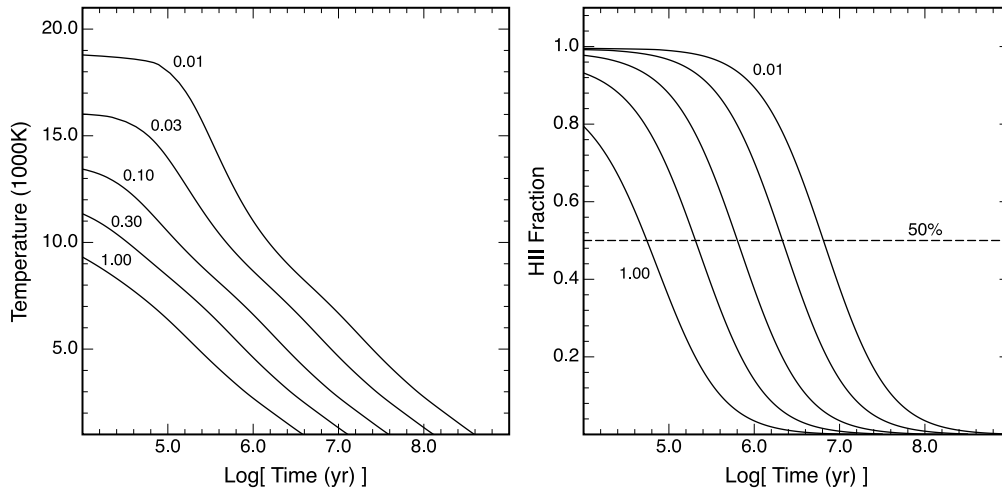


FIG. 5.— *MAPPINGS IV* time-dependent calculations of how the ionised surface of a dense gas clouds cools with time: (Left) electron temperature T_e ; (Right) ionisation fraction χ . We show the isochoric (constant density) models where the densities in cm^{-3} are indicated; isobaric models cool twice as fast at late times. The $H\text{I}$ clouds have 0.1 Z_\odot metallicity and are irradiated at $D = 55$ kpc by an AGN accretion disk ($f_E = 0.1$) at the Galactic Centre (Fig. 3).

At late times, the $H\alpha$ surface brightness in all cases scales as t^{-2} ; see Appendix A.

In Table 1, we show key properties of the models as a function of the pre-ionisation gas densities. The realistic cases are shown as emboldened values where we have ignored small factor uncertainties; the remaining models exceed the properties (either local or column density) of the Stream clouds. Column 5 shows the times T_d for the emission to drop to the canonical surface brightness of 160 mR (see Fig. 2). The look-back times are shown in Column 6; note that the light propagation time ($2T_C$) dominates the high density extremes. These timescales are in line with published models of the Fermi bubbles (§1). The lower ionising flux at the 100 kpc distance (since the peak luminosity in the models is fixed) leads to shorter look-back times because the gas requires less time to reach 160 mR.

Distance vs. Flare Luminosity. It is clear from Fig. 4 that

lower ionising fluxes or larger Stream distances lead to shorter inferred timescales for the Seyfert flare event. To within a small factor, the ionisation model (D, f_E) = (55 kpc, 0.1) is equivalent to the (100 kpc, 0.3) model once all timescales are considered. Conversely, the ionisation model (D, f_E) = (100 kpc, 0.1) is equivalent to the (55 kpc, 0.03) model. In Appendix A, we present a simplified model for the evolution of the ionisation fraction and $H\alpha$ surface brightness from the Stream which is in good agreement with the *MAPPINGS* models shown in Fig. 4, which we use to discuss in more detail the constraints that can be placed on the flare energetics and evolution in §5.1.

Variations in $H\alpha$ brightness. An attractive aspect of the Seyfert flare model is the ability to accommodate the brightest $H\alpha$ measurements and the scatter about the elevated mean surface brightness (160 mR) compared to the expective Galactic ionisation level. An interesting question is whether the scatter

TABLE 1
MAPPINGS IV TIME-DEPENDENT IONISATION CALCULATIONS^a

^aSeyfert flare model ($f_E = 0.1$) using two distances ($D = 55, 100$ kpc) for the Magellanic Stream. The columns are: (1) hydrogen gas density; (2) depth of ionised layer integrated to 90% neutral; (3) $H\alpha$ surface brightness in $\text{erg cm}^{-2} \text{s}^{-1} \text{arcsec}^{-2}$; (4) $H\alpha$ surface brightness in mR; (5) time for the ionised gas to cool down to $\mathcal{E}_m = 160$ mR; (6) look-back time $T_o = T_R +$ twice the light propagation time (T_C). Emboldened rows are consistent with the known gas properties of the Stream.

(a) 55 kpc					
$n_H(\text{cm}^{-3})$	$d_m(\text{pc})$	$\mu_{H\alpha}(\text{cgs})$	$\mu_{H\alpha}(\text{mR})$	$T_R(\text{yr})$	$T_o(\text{yr})$
1.0	9	4.8e-18	844	1.3e5	4.9e5
0.3	63	4.8e-18	848	4.3e5	7.9e5
0.1	404	4.8e-18	849	1.4e6	1.8e6
0.08	1423	4.8e-18	852	1.8e6	2.9e6
0.03	3461	4.9e-18	858	4.7e6	5.1e6
(b) 100 kpc					
$n_H(\text{cm}^{-3})$	$d_m(\text{pc})$	$\mu_{H\alpha}(\text{cgs})$	$\mu_{H\alpha}(\text{mR})$	$T_R(\text{yr})$	$T_o(\text{yr})$
1.0	4	1.4e-18	251	3.0e4	7.5e5
0.3	31	1.5e-18	258	1.0e5	8.2e5
0.1	178	1.5e-18	258	3.2e5	1.0e6
0.03	1345	1.5e-18	257	1.2e6	1.9e6
0.01	9230	1.5e-18	259	4.2e6	4.9e6

reflects variations in gas density (geometry) or photon arrival time (finite T_B). In Fig. 6, we show the relation between $\mu_{H\alpha}$ and n_H at a fixed time over a range of times from 0.5 Myr to 5 Myr. For an impulsive burst, it is possible to accommodate all of the detections at a fixed time, certainly within the first few Myr of the Seyfert event. But the very short ionisation timescale T_I (§3.1) means that we are unlikely to see temporal variations of the source: the Stream emission is unaffected by any variations in incident ionising flux that occurred longer than $\sim T_I$ ago. Source luminosity variations on longer timescales will be modulated by a transfer function that depends on the gas density (see Appendix A); any observable fluctuations in $H\alpha$ are likely the result of variations in density and hence recombination timescale. The most relevant epoch in interpreting the Stream emission is the end of the flare.

From the last column in Table 1, we conclude that a powerful flare event occurred 1–3 Myr ago. The inferred magnitude of the event depends on a number of factors, in particular, the poorly constrained distance to the Magellanic Stream (see §5 and Appendix A), but it must have been at levels associated with the most energetic Seyfert activity ($f_E > 0.01$).

4. FUTURE TESTS OF THE MODEL

In Seyferts with moderately low mass black holes, the jet/wind/cone axis can be strongly misaligned with the spin axis of the galaxy (Cecil 1988; Mulchaey et al 1996) but there are many counter examples (Duric et al 1983; Wehrle & Morris 1987, 1988; Keel et al 2006). The Fermi bubbles and the X-ray bipolar structure are roughly aligned with the SGP. These features fill most of the conic volume in our model within 10 kpc, and presumably the outflow has swept any halo gas aside. We assume that the ionisation cone in the Seyfert flare model is also aligned with the SGP ($\ell_M \approx 303^\circ$). Thus to account for the brightest clouds in the Stream (Fig. 2), the half-opening angle $\theta_{1/2}$ of the cone is at least 25° to accommodate enhanced emission at the same angle from the SGP ($\ell_M \approx 278^\circ$).

Any gas clouds caught within the cones at smaller distances

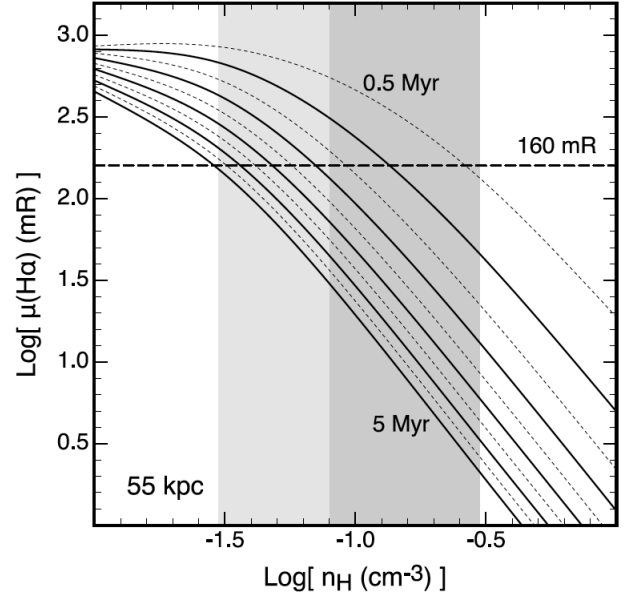


FIG. 6.— MAPPINGS IV time-dependent isochoric calculations of the change in $H\alpha$ surface brightness after a Seyfert flare has occurred at the Galactic Centre ($D = 55$ kpc, $f_E = 0.1$; $Z = 0.1 Z_\odot$). The canonical Stream brightness (160 mR) is shown as a horizontal dashed line. The tracks plotted every 0.5 Myr show the relation between $H\alpha$ and gas density at a fixed recombination time T_R . The associated look-back times (offset by the light crossing time) are shown in Table 1. The dark vertical band shows the range in n_H consistent with the known cloud properties; the lighter band is marginally consistent.

will be roasted by the Seyfert nucleus. However, almost all the known high velocity clouds reside close to the Galactic Plane ($b < 30^\circ$; Putman et al 2012). There are few known HVCs close to the SGP although evidence for ionised HVCs has been presented (Lehner & Howk 2010). In our model, most of the HVCs will be fully ionised within the ionisation cone. Interestingly, there is one sight line close to $\ell_M = 308^\circ$ where the $H\alpha$ surface brightness is up to 4 times higher than our benchmark flare value of 160 mR (Fig. 2). A possible explanation is that some of the Stream clouds are somewhat closer than the canonical distance of 55 kpc.

A competing model for the $H\alpha$ emission uses a radiative hydrodynamic simulation to demonstrate the possibility of a slow shock cascade acting along the Stream (Bland-Hawthorn et al 2007). Arguably, this is the *only* serious attempt to date to explain the Stream $H\alpha$ emission. But this model *does not* work well if the Stream at the SGP is at the larger distance of $D \approx 100$ kpc. Given that one end (front) of the Stream is tied to the LMC-SMC system, this would require the far trailing end (back) of the Stream to subtend a large angle to the halo, being more radial than tangential to the halo. This has two problems: (i) the $H\alpha$ emission would be almost entirely confined to the front of the Stream; (ii) the back of the Stream would be undetectable.

For the near distance of $D = 55$ kpc, for most optical diagnostics, the slow shock cascade may be difficult to disentangle or distinguish from our model of AGN photoionisation. The diluteness of the predicted AGN field, with ionisation parameters in the range $\log q = 5.6 - 7.6$ ($\log u \approx -5$ to -3), tends to produce shock-like emission line diagnostics. The high energy part of the big blue bump (50–100 eV) can excite He II and [O III], with enhanced ratios to $H\beta$ of about 0.3 and 1 respectively. But these occur at the peak of the flash and fade rapidly, and only for the near-field Stream (Fig. 4a). The high

energy tail in eq. (7) can excite a few atoms with high ionisation cross sections but the radiation field in X-rays is very dilute, and the metal fraction is low ($[\text{Fe}/\text{H}] \approx -1$; Fox et al 2013).

We are presently re-running the shock cascade models at higher resolution and with the updated ionisation diagnostics in *MAPPINGS IV*. This will be the focus of a later paper. The shock cascade has a slightly elevated density-weighted temperature ($T_e \gtrsim 12,000$ K) compared to the time-averaged Seyfert flare model ($T_e \approx 10,000$ K). But both models produce comparable emission in the optical diagnostic $[\text{S II}]$, $[\text{N II}]$ and $[\text{O I}]$ emission lines.

A promising diagnostic is the Balmer decrement $\text{H}\alpha/\text{H}\beta$ which is typically enhanced in slow shock models (Bland-Hawthorn et al 2007). The dust content in the Magellanic Stream has negligible impact on this line ratio. Diffuse optical detection surveys to date have largely focussed on the 500–700 nm window in part because $\text{H}\beta$ is harder to detect along most of the Stream (Reynolds et al 1998). In our Seyfert flare models, the Balmer decrement at the distance of the Stream is in the range 3.0–3.1 for detectable emission, rising slowly at late times when the recombination emission has largely faded. In the shock cascade model, the Balmer decrement exceeds 3.1 and can reach values that are 50% higher.

5. NEW INSIGHTS ON AGN ACTIVITY

5.1. Accretion disk

Sgr A* provides us with a front-row seat on the daily life of a supermassive black hole⁴. Nuclear activity today at the Galactic Centre is remarkably quiescent given the rich supply of unstable gas within the circumnuclear disk (Requena-Torres et al 2012). This observation has driven the rapid development of accretion disk models over the past twenty years: a comprehensive review is given by Genzel et al (2010). It is now believed that Sgr A* is a radiatively inefficient accretion flow (RIAF) fuelled by poor angular momentum transport at all radii in part due to strong outflows, magnetic fields and convection in the innermost accretion zone (Blandford & Begelman 1999; Hawley & Balbus 2002; cf. Jolley & Kuncic 2008).

The observed material within a few parsecs of Sgr A* can readily account for the $0.02 - 0.2 M_\odot \text{ yr}^{-1}$ accretion rate required in our model. Stellar accretion events are expected once every 40,000 years on average (Freitag et al 2006). There are indications of infalling gas clouds over the past 10 Myr. One such cloud impact possibly triggered the formation of a kinematically distinct $\sim 10^4 M_\odot$ cluster within ~ 0.1 pc of Sgr A*, traced by ~ 80 massive young stars with ages in the range 2.5 – 8 Myr (Paumard et al 2006; Lu et al 2013). Wardle & Yusef-Zadeh (2008) draw attention to the “+50 km s⁻¹ cloud” known to have passed through the Galactic Centre within the last 1 Myr. These events bracket our inferred epoch for the Seyfert flare which may have been causally linked to one of these or a related event.

We do not know what the peak luminosity of the AGN burst was, or the timescale on which it decayed. Such information would shed light on the nature of the accretion event, whether an individual star ($T_B \sim 10^{2-3}$ yr) or an infalling cloud on

much longer timescales. However, we can use the simplified model for the Stream emission developed in Appendix A, which is in good agreement with the detailed *MAPPINGS IV* results for the time-dependent $\text{H}\alpha$ surface brightness, to place constraints on these quantities.

As in Appendix A, define ρ to be the ratio of the observed $\mu_{\text{H}\alpha}$ to its peak value. This is also equal to the ratio of the minimum required ionizing flux (eq. [2]) or ionizing luminosity (eq. [3]), to their peak values, as well as the minimum required value of the Eddington fraction $f_{E,\text{min}}$ to its peak during the burst. Using eq. (2) and eq. (12) for the ionizing flux from the AGN (with $f_{\bullet,\text{esc}}$ set to 1), we can write this minimum Eddington fraction as

$$f_{E,\text{min}} = 0.02 \left(\frac{D}{55 \text{ kpc}} \right)^2 \quad (14)$$

In the limit where the e -folding time for decay of the burst τ_s is much shorter than the recombination timescale τ_{rec} , we have the analytic result

$$f_{E,\text{peak}} = f_{E,\text{min}} (1 + \tau_o)^2 \quad (15)$$

where τ_o is the dimensionless age of the burst as measured in recombination times. (This is simply another form of eq. [A23]). Using eq. (A9) for τ_{rec} and eq. (14) for $f_{E,\text{min}}$, we have calculated the required peak value of f_E as a function of gas density n_H and burst age T_o , for both $D = 55$ kpc and 100 kpc. Assuming that the present-day Eddington fraction of Sgr A* is $\sim 10^{-8}$ (Genzel et al 2010), we can also calculate the required value of the e -folding time τ_s : the inferred value of peak f_E at a given T_o determines the number of e -folding times that have passed in the age of the burst.

The results are shown in Fig. 7. The grey upper right portion of the diagrams is where $f_{E,\text{peak}}$ exceeds 1; this occurs sooner at higher n_H (more recombination times) and larger T_o (more e -folding times τ_s). This condition is violated more readily for $D = 100$ kpc, since a greater φ_i is needed to produce the same $\text{H}\alpha$ surface brightness; this also means the minimum allowed value of f_E is ~ 3.3 times larger. However, a broad range of reasonable f_E is allowed for burst ages greater than ~ 1 Myr in both cases; a larger Stream distance favors lower n_H (to increase τ_{rec}) and larger $f_{E,\text{peak}}$.

Although we have assumed that $\tau_s \rightarrow 0$ in Fig. 7, the results are not very sensitive to this assumption: in Appendix A, we show that τ_{rec}/τ_s is likely to be a factor of order a few; for these values, there are modest shifts of the curves from the instantaneous decline case (see Fig. 10 in Appendix A).

In our interpretation, Sgr A* was far more active in the past. Rapid and stochastic variations in AGN activity are to be expected (Novak et al 2011, 2012). Depending on the Stream distance, for plausible n_H and T_o the required Eddington fraction f_E is of order $0.03 - 0.3$ which is a factor of 10^{7-8} times higher than the quiescent state today.⁵ The most extreme event witnessed in models by Novak et al (2011, their Fig. 6) is a transition from $f_E \sim 10^{-3}$ to $f_E \sim 3 \times 10^{-8}$ in a few Myr (45 dB). This happens when there is a lot of material in the accretion disk around the black hole. The AGN heats up the ISM and terminates additional infall, and then the mass drains out of the disk with an e -folding time of about 0.1 Myr.

⁴ <http://swift-sgra.com> provides regular updates on energetic episodes at the Galactic Centre. At the time of writing, much interest has been sparked by the anticipated “G2 cloud” collision – a warm cloud of several Earth masses – expected to occur in 2014 (Gillessen et al 2013).

⁵ While such an event would be spectacular to behold using modern astronomical techniques, to an ancient observer, escaping shafts of light that managed to pierce through the heavy dust obscuration towards Earth would have been at least an order of magnitude fainter than the full moon.

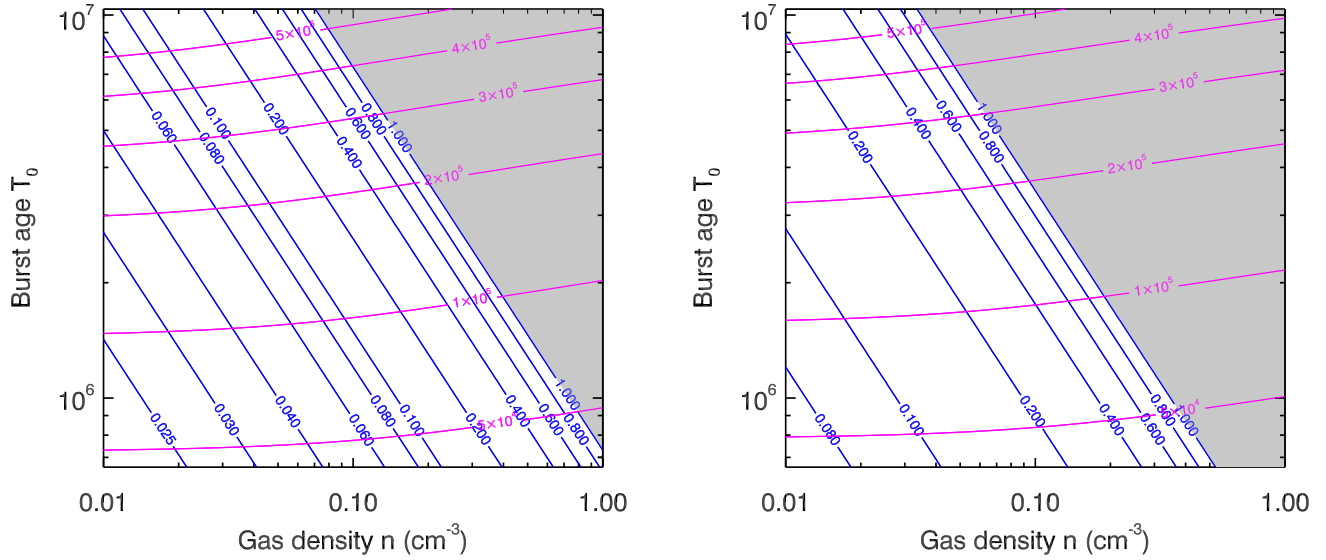


FIG. 7.— The constraints on the Sgr A* burst peak Eddington fraction $f_{E,\text{peak}}$ (blue contours) and burst decay e -folding time τ_s (magenta contours) as a function of Stream gas density n_H and burst age T_0 , for the case of very rapid burst decline. The grayed-out region requires $f_E > 1$. (Left): $D = 55$ kpc. (Right): $D = 100$ kpc.

The timescale of the drop is roughly the characteristic time to clear the accretion disk (G. Novak, private communication).

But our new result demands 70-80 dB suppression within a time frame of only $\sim 1-5$ Myr. Such a rapid variation requires an extremely efficient and well confined ‘drip line’ to prevent the fresh gas from being sheared by the accretion disk which would wash out extreme fluctuations in UV luminosity (S. Balbus, private communication). Magnetic fields – required to mediate angular momentum transport – are expected to thread through a RIAF disk and these are almost certainly needed to achieve the severe confinement and rapid fuelling.

In time, we may learn about the detailed structure of the evolving accretion disk before, during and after a major outburst (Ho 2008). If the Seyfert flare model is ultimately confirmed to be the correct explanation for the Stream’s partial ionisation, it provides us with a very interesting and spatially resolved probe of the escaping radiation. We refrain from considering more sophisticated accretion disk/jet models, with their attendant beaming, until more progress is made in establishing the true source of the ionising radiation and the Stream’s trajectory. A stronger case must be made for preferring this model over another (i.e. the shock cascade). But we note that the green horizontal line in Fig. 2 is not a good fit to most of the data points. An inverted low amplitude parabola centred on the SGP does better. This can be understood in terms of an accretion disk radiation field with a polar angle component; such models have been presented (e.g. Madau 1988; Sim et al 2010). But the trend to lower Magellanic longitude conceivably can be explained if the Stream subtends a large angle to the Galactic halo.

5.2. UV line-driven wind

It is evident that the explosive nuclear activity that created the extended X-ray, microwave and gamma-ray radiation gave rise to a large-scale outflow from the Galactic Centre. Both starburst and AGN activity are likely to be operating from the central regions. While their time-averaged en-

ergetic outputs may be similar, they operate with very different duty cycles and temporal behaviour (Alexander & Hickox 2012). The Fermi observations have been discussed extensively in the context of accretion disk activity associated with the well established supermassive black hole (Su et al 2010; Guo & Mathews 2012) although alternative starburst models have been presented (Carretti et al 2013). Starbursts drive large-scale winds very effectively and may assist with the observed bipolar activity. But as already mentioned (§1; see also Appendix B), starburst activity cannot account for the Stream H α emission.

Is it possible to associate the powerful radiative phase with the wind phase? Regrettably, there are few published accretion disk models that provide both the ionising luminosity and mechanical luminosity of the central source. For our discussion, we use the well prescribed models of Proga & Kallman (2004; hereafter P-K) that build on their earlier work (Proga, Stone & Kallman 2000).

In the P-K wind models, the relatively high radiation UV flux and opacity (mainly due to line transitions) supply a strong radiative force that is able to lift gas over the photosphere. This gas provides significant column density to block the X-rays otherwise the wind becomes overionised and the flow switches off. The line-driven wind is launched from the part of the disk where most of the UV is emitted. In effect, the inner disk wind shields the outer wind. The high value of η in eq. (7) is consistent with our assumption that the UV radiation dominates over X-rays and powers the large-scale wind (Proga, Stone & Kallman 2000).

The P-K wind reaches velocities roughly twice the escape velocity from the launching region. So this gives velocities of about 10,000 km s $^{-1}$ for a system with $M_\bullet = 10^8 M_\odot$ although maybe somewhat less for the supermassive black hole associated with the Galactic Centre. With this velocity it will take only 0.1 Myr to reach a distance of 1 kpc, and 1 Myr to reach 10 kpc. The disk wind mass loss rate is roughly 10% or so of the disk accretion rate and therefore does not cause a signif-

icant reduction of the accretion rate. The wind is unlikely to ionise cold gas at the distance of the Stream.

Using the Proga models, Sim et al (2010) computed spectral energy distributions as a function of viewing angle as seen from the accretion disk. They compute the photoionisation and excitation structure of the wind and track multiple scattering of the photons. The polar radiation field depends on photon energy and the escaping radiation is confined to a cone. The X-ray and the UV radiation come from different directions; the former propagate parallel to the UV photosphere whereas the latter is normal to it. Therefore the column density for the X-rays is much higher than for the UV as expected, although some leakage is observed.

We observe that something like this may be happening in detailed observations of nearby active galaxies. In an integral field study of ten galactic winds, Sharp & Bland-Hawthorn (2010) compared five starbursts and five AGNs. The AGN winds show clear evidence for non-thermal ionisation from the central source across the wind filaments to the radial limits of the data. But AGN ionisation cones are not always associated with winds. For example, the most famous of the Seyfert ionisation cones is NGC 5252 (Tadhunter & Tsvetanov 1989) which is not associated with an energetic outflow. In the context of the P-K model, we associate these cones with AGNs where strong X-rays escape from the nucleus which serve to suppress the line-driven wind. This distinction may become less clear cut if more powerful line-driven winds (presumably from more massive black holes) are able to drive shocks in the gas along the ionisation cone. Thus ionisation cones may be detectable in X-rays even while the central source irradiates the cone exclusively with UV. Shocked gas tends to radiate at a higher temperature compared to photoionised gas, and this may allow these cases to be separated.

Line-driven winds struggle with black hole masses as low as that associated with Sgr A* unless the accretion rate is close to the Eddington limit. If the Stream ionisation is due to a burst of radiation from a P-K disk, then $f_E \sim 1$ is an order of magnitude more than is need to account for the observed $H\alpha$ emission for the canonical Stream distance (55 kpc), although it would aid ionisation of the Stream at the larger distance. In principle, $f_{\bullet, \text{esc}}$ could be lower than our assumed value of 100%. But the high limit is consistent with what we know about ionisation cones (e.g. Mulchaey et al 1996) and is a consequence of the P-K wind model where the wind has cleared a channel for the UV emission (Proga & Kallman 2004; Sim et al 2010).

6. CONCLUSIONS

We have shown how the Magellanic Stream is lit up in optical emission lines at a level that cannot be explained by disk or halo sources. A possible explanation is a shock cascade caused by the break-up of clouds and internal collisions along the Stream (Bland-Hawthorn et al 2007) but this becomes untenable if the Stream is much further than the canonical distance of 55 kpc.

We have introduced time-dependent ionisation calculations with *MAPPINGS IV* for the first time in order to present a promising Seyfert flare model that adequately explains the observed photoionisation levels along the Magellanic Stream. The model works at both the near and far Stream distances, and can be tested in future observations. A ‘slow shock cascade’ is expected to produce a steeper Balmer decrement ($H\alpha/H\beta > 3.1$) than the flare model. Since the Magellanic Stream has a very low dust fraction ($[Fe/H] \approx -1$), this is likely

to be the most accessible discriminant between the models. Other useful diagnostics ($He II/H\beta$, $[O III]/H\beta$) reach peak values shortly after the Seyfert flash but fade rapidly.

We cannot yet identify the specific event which triggered the burst of Seyfert activity although the stellar record tells us the past 10 Myr have been very active (Ponti et al 2013). The time lag between an accretion event and the onset of starburst or AGN activity (or how these operate together) is a major unsolved problem in astrophysics. The inner tens of parsecs provide many possible cloud candidates, assuming it was not largely consumed, many on highly elliptic orbits. If our model is correct, it provides many new challenges for the burgeoning field of Galactic Centre research. Regardless of the origin of the emission, the Stream provides an important constraint on past AGN activity and on models that attempt to explain the *Fermi* gamma-ray bubbles.

7. ACKNOWLEDGMENT

This work came about during the April 2013 ‘Fermi Bubbles’ workshop held at KIPAC Stanford organised by Dmitry Malyshev and Anna Frankowiac. We acknowledge insightful conversations with Steve Balbus, Bill Mathews, Daniel Proga, Greg Novak, Bruce Draine and Kyler Kuehn. JBH is indebted to James Binney for early comments on the manuscript. We are particularly grateful to Roger Blandford and the participants of the Kavli workshop without whom this paper may not have been realised. We thank the referee for suggestions that led to more detailed discussions in the appendix.

APPENDIX

A. A SIMPLE MODEL FOR TIME-DEPENDENT EVOLUTION OF THE IONISATION FRACTION AND H α SURFACE BRIGHTNESS

Consider the following simple model for the Stream clouds: a uniform density gas of pure hydrogen, with a photon flux φ_i normally incident upon it. If the gas has been exposed to the ionising photons for long enough to reach ionisation equilibrium, then all of the photons will be absorbed in a length L given by

$$\alpha n_e^2 L = \varphi_i \quad (\text{A1})$$

where α is the recombination coefficient. This is just the condition that the column recombination rate equals the incident flux. Thus

$$L = \frac{\varphi_i}{\alpha n_e^2} \quad (\text{A2})$$

To simplify even further, assume that for depth $d < L$ into the Stream gas, the gas is completely ionised, while for $d > L$, it is neutral. Hence all the emission measure comes from $d < L$, and we will also ignore any effects of absorption on φ_i , so the region with $d < L$ can be treated as uniform.

Now suppose that the ionisation rate decreases from the initial value for which the equilibrium was established. Without loss of generality, we can assume an exponential decline for φ_i , with a characteristic timescale for the ionising source τ_s (Sharp & Bland-Hawthorn 2010). The time-dependent equation for the electron fraction $x_e = n_e/n_H$ is

$$\begin{aligned} \frac{dx_e}{dt} &= -\alpha n_H x_e^2 - \zeta x_e + \zeta \\ &= -\alpha n_H x_e^2 + \zeta_0 e^{-t/\tau_s} (1 - x_e) \end{aligned} \quad (\text{A3})$$

where ζ is the ionisation rate per atom.

Consider first the case where $\tau_s \rightarrow 0$, so that φ_i declines instantaneously to zero. Then the second and third terms in eq. (A3) vanish, and we just have

$$\frac{dx_e}{dt} = -\alpha n_H x_e^2 \quad (\text{A4})$$

This is easily solved with the substitution $u = x_e^{-1}$, and with the initial condition $x_e = 1$ at $t = 0$ we get

$$x_e = \frac{1}{1 + \alpha n_H t} \quad (\text{A5})$$

Defining the recombination timescale

$$\tau_{\text{rec}} = 1/\alpha n_H \quad (\text{A6})$$

this is simply

$$x_e = (1 + t/\tau_{\text{rec}})^{-1} \quad (\text{A7})$$

To evaluate eq. (A7) for the conditions in the Stream, we use $\alpha_B = 2.6 \times 10^{-13} \text{ cm}^3 \text{ s}^{-1}$ for the recombination coefficient (appropriate for hydrogen at 10^4 K), and use the fiducial values $\varphi_i = 10^6 \varphi_6 \text{ phot s}^{-1}$, $n_H = 0.1 n_{-1} \text{ cm}^{-3}$. Then

$$L = 125 \frac{\varphi_6}{n_{-1}^2} \text{ pc} \quad (\text{A8})$$

$$\tau_{\text{rec}} = 1.2 \times 10^6 / n_{-1} \text{ yr} \quad (\text{A9})$$

and the emission measure

$$\mathcal{E}_m = L n^2 x_e^2 = 1.25 \varphi_6 x_e^2(t) \text{ cm}^{-6} \text{ pc} \quad (\text{A10})$$

so the gas density enters explicitly only through the recombination time. The resulting H α emission will be

$$\mu_{\text{H}\alpha} = 413 \varphi_6 x_e^2(t) \text{ mR} \quad (\text{A11})$$

or, with eq. (A7)

$$\mu_{\text{H}\alpha} = 413 \varphi_6 (1 + t/\tau_{\text{rec}})^{-2} \text{ mR} \quad (\text{A12})$$

In the lefthand panel of Fig. 8, we plot the prediction of eq. (A12) for the H α surface brightness as a function of time for $\varphi_6 = 2$, as used in eqs. (10) and (11) for $D = 55 \text{ kpc}$. Comparison with the left-hand panel of Fig. 4 shows that this simple model agrees well with the detailed MAPPINGS results, except for the highest densities. The discrepancy is largely because eq. (A12) predicts that x_e depends only on t/τ_{rec} , and hence x_e remains close to unity (and thus $\mu_{\text{H}\alpha}$ at its peak value) only if t/τ_{rec} is small, but that is not true for the highest densities at the earliest times for the range of times that are plotted. However, it clearly does a good job of reproducing the late-time behaviour ($\mu_{\text{H}\alpha} \propto (t/\tau_{\text{rec}})^{-2}$), to which all the models in Fig. 4 asymptote.

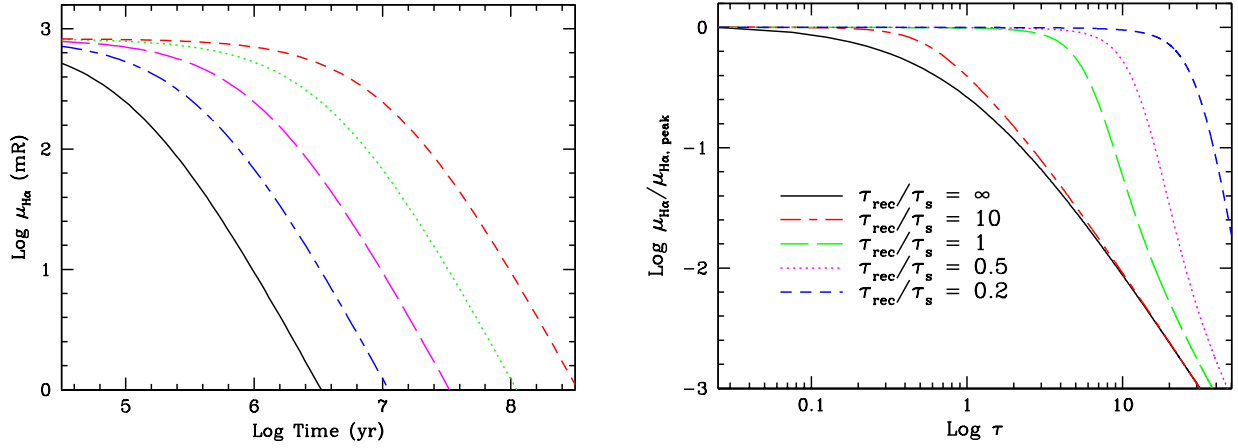


FIG. 8.— (Left) The $H\alpha$ surface brightness as a function of time predicted by eq. (A12), for $\varphi_6 = 2$. From left to right, the curves are for gas density $n_H = 1, 0.3, 0.1, 0.03$, and 0.01 cm^{-3} . (Right) The evolution of the $H\alpha$ surface brightness (scaled to the peak brightness) with dimensionless time τ obtained by solving eq. (A16) for several values of the ratio β of recombination time to ionising photon flux decay time. Curves are labeled with β ; all models assume a ratio of recombination time to “ $t = 0$ ionisation time,” $\gamma = \tau_{\text{rec}}/\tau_i^0 = 240$.

Equation (A3) does not have an analytic solution when the time-dependence of φ_i is included. However, it is easily solved numerically and can be transformed into a more useful form with some trivial definitions. Define the dimensionless time τ by

$$\tau \equiv \alpha n_H t = t/\tau_{\text{rec}}; \quad (\text{A13})$$

τ is simply the time measured in units of the recombination time. In addition, define

$$\gamma = \tau_{\text{rec}}/\tau_i^0 \quad (\text{A14})$$

where τ_i^0 is the ionisation time at $t = 0$, and

$$\beta = \tau_{\text{rec}}/\tau_s, \quad (\text{A15})$$

the ratio of recombination to ionising photon luminosity e -folding times. Then eq. (A3) becomes

$$\frac{dx_e}{d\tau} = -x_e^2 + \gamma e^{-\beta\tau}(1-x_e) \quad (\text{A16})$$

We can write the ionisation rate per H atom as

$$\zeta \simeq C_i \varphi_i \sigma_0 \quad (\text{A17})$$

where σ_0 is the H ionisation cross-section at threshold and C_i is a constant of order unity that depends on the shape of the spectrum. The ionisation time τ_i^0 then evaluates to

$$\tau_i^0 = 5000 \frac{C_i}{\varphi_6} \text{ yr} \quad (\text{A18})$$

and we can write γ as (using eq. [A9] for τ_{rec})

$$\gamma = 240 \frac{\varphi_6}{C_i n_{-1}} \quad (\text{A19})$$

The resulting $H\alpha$ surface brightness obtained from the solution of eq. (A16) for the ionisation fraction, normalized to the peak value, is shown in the righthand panel of Fig. 8 for $\gamma = 240$ and values of β from 0.2 to ∞ ($\tau_s \rightarrow 0$, the case shown in the lefthand panel). However, an important point from this analysis can be derived simply from the form of eq. (A16). As just shown, γ must be large – this is inevitable from the assumption that the gas in the $H\alpha$ -emitting region is highly ionised to begin with. Hence the ionisation fraction (and thus the $H\alpha$ surface brightness) will not begin to decrease substantially until

$$e^{-\beta\tau} \sim 1/\gamma \quad (\text{A20})$$

and thus until τ reaches the critical value

$$\tau_c \sim \frac{\ln \gamma}{\beta}. \quad (\text{A21})$$

Physically, this is just a reflection of the requirement that the ionisation time must be longer than the recombination time before the ionisation fraction begins to drop. If $\beta \lesssim 1$ — the ionising photon flux is decreasing on a timescale longer than the recombination timescale — the ionisation fraction (and thus the $H\alpha$ emission) will not begin to decline substantially until many recombination times have passed.

The numerical solutions of eq. (A16) show that the expression (A21) for the critical time is quite accurate: for $\gamma = 240$, it predicts $\tau_c \sim 0.55, 5.5, 11$, and 27 for $\beta = 10, 1, 0.5$, and 0.2 , respectively. Since τ_c depends only logarithmically on φ_i and the gas density n_H , the precise values of these quantities are unimportant — all that matters is that, generically, $\ln \gamma \sim$ a few. Unless τ_s is much shorter than τ_{rec} ($\beta \gg 1$), the decline of x_e — and thus of $\mu_{\text{H}\alpha}$ — is substantially delayed from the instantaneous φ_i turn-off case. (Note also that for $\beta < 1$, the decline is steeper once it begins. This is because the derivative of x_e with respect to $\ln \tau$ has its maximum at τ_c — physically, there is simply more time available between the steps of $\ln \tau$ at these later times.)

This simple model can also be used to address another very important issue. We do not know *a priori* what the peak luminosity of the burst was, or the timescale on which it decayed. All we know is that the peak H α surface brightness was at least equal to the present-epoch value. Define

$$\rho = \mu_{\text{H}\alpha, \text{obs}} / \mu_{\text{H}\alpha, \text{peak}} \quad (\text{A22})$$

which is also equal to the ratio of minimum to peak ionizing photon luminosity $N_{i, \text{min}} / N_{i, \text{peak}}$ and to the ratio of the minimum required Eddington fraction to the peak value, $f_{E, \text{min}} / f_{E, \text{peak}}$. Consider first the limit of $\tau_s \rightarrow 0$. From eq. (A7), we have

$$\rho = (1 + t / \tau_{\text{rec}})^{-2} \quad (\text{A23})$$

(cf. eq. [A12]). The time needed for the H α surface brightness to decline to its observed value, in units of the recombination time, is simply

$$\tau_\rho = \rho^{-1/2} - 1 \quad (\text{A24})$$

The value of τ_ρ predicted by eq. (A24) agrees reasonably well with the models presented in Fig. 4. For $D = 55$ kpc, $\rho \simeq 0.2$, and so $\tau_\rho = 1.24$. Using eq. (A9) for τ_{rec} , the values from Table 1 give $\tau_\rho = 1.08 - 1.2$, while for the $D = 100$ kpc model, $\rho \simeq 0.64$, so the predicted value of $\tau_\rho = 0.25$, while the derived values range from 0.25 to 0.35. The differences between the prediction and the calculated values result from the simplification of eq. (A9) in assuming a constant recombination coefficient that is independent of time and ignores the different temperature histories as shown in Fig. 5.

For the case of non-instantaneous decline of the burst luminosity, we can easily solve for τ_ρ numerically for different values of β . One difference from the results shown in the righthand panel of Fig. 8 is that we must define γ consistently with the choice of ρ ; this can be seen by noting that eq. (A14) for γ can be written, using eq. (2) for $\varphi_{i, \text{min}}$ and eq. (A9) for τ_{rec} , as

$$\gamma = \frac{93.6}{\rho n_{-1}} \quad (\text{A25})$$

which we use to specify γ as a function of ρ .

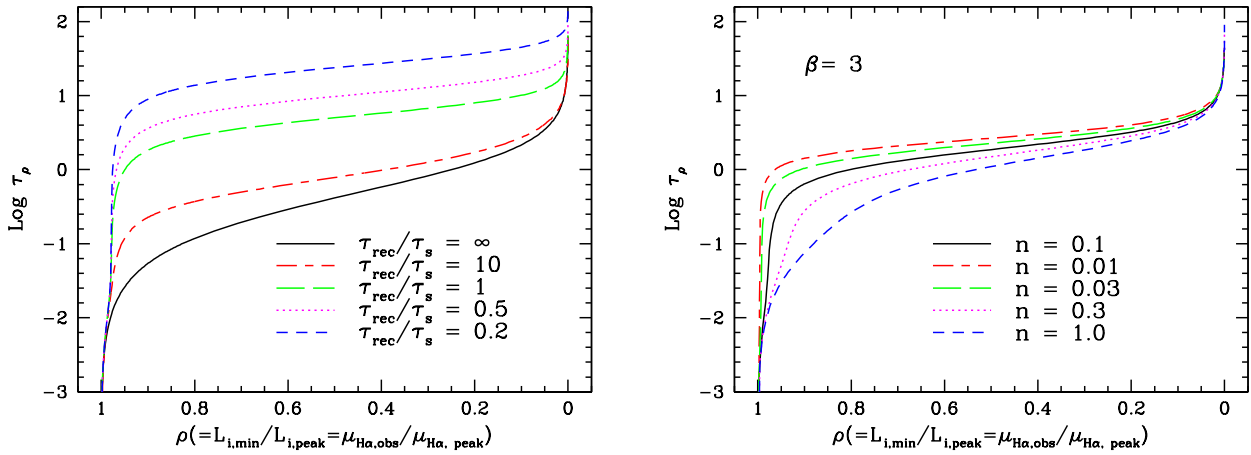


FIG. 9.— (Left) The dimensionless time τ required for the H α surface brightness to decline to a fraction ρ of its peak value; ρ is also equal to the ratio of the minimum ionizing photon flux or luminosity to their respective peak values. Curves are labeled with β , the ratio of recombination time to ionising photon flux decay time. A Stream gas density of $n_H = 0.1 \text{ cm}^{-3}$ was assumed. (Right) As in the left panel, except for β fixed at 3 and different values of the gas density (labeled).

The solutions for τ_ρ are shown in Fig. 9. The left panel assumes a Stream gas density fixed at $n_H = 0.1 \text{ cm}^{-3}$, and shows the results for several different values of β (as in Fig. 7). The offset between the curves with different β is a direct reflection of the delay in the decline of $\mu_{\text{H}\alpha}$ seen in the righthand panel of Fig. 8. In the righthand panel of Fig. 9, β has been fixed at 3 (see below), and τ_ρ is plotted against ρ for several different densities. From eq. (A25), for fixed ρ the value of γ increases with decreasing density n_H , which is why the curves flatten out as n_H declines to the lowest values. The spread is much smaller than in the variable- β curves shown in the lefthand panel, especially for small values of ρ ; this is because τ_c depends only on $\ln \gamma$ whereas it depends linearly on $1/\beta$, as discussed above (eq. [A21]). The steep decline as $\rho \rightarrow 1$ seen in both panels of Fig. 10

is imposed by the initial condition $x_e = 1$ at $\rho = 1$. The convergence of all the models to the same steep rise as $\rho \rightarrow 0$ results from the negligible size of the ionization term at late times ($\tau \gg \tau_c$), so that they all approach the $x_e \propto \tau^{-2}$ solution (A7) for the instantaneous-decline case.

We use these results in §5.1 to discuss the constraints on the peak luminosity and decay timescale of the Sgr A* flare. Here we note that β is likely to be at least a few. In terms of the Eddington fraction and the burst age T_o , we can evaluate eq. (A24) to get

$$n_H T_o \lesssim 1.2 \times 10^5 \left(\frac{7.1}{(D/55 \text{ kpc})} - 1 \right) \text{ cm}^{-3} \text{ yr} \quad (\text{A26})$$

for $f_{E,\text{peak}} = 1$. This gives the largest possible value for τ_s . In §5.1, we infer a central flare that has faded by 80 dB, or approximately 18 e -folding times, since the burst peak. With eq. (A26), we then get that $\tau_s \lesssim 4(2) \times 10^5 / n_H$ for $D = 55(100)$ kpc. This implies $\beta \gtrsim 3-6$ for the Stream distances: burst decay times longer than $\tau_s \sim \text{a few} \times 10^5$ yr are unlikely, given the probable age of the *Fermi* bubbles. In Fig. 10 we show the required value of Eddington fraction f_E as a function of burst age T_o and gas density n_H for these two cases. Comparison with Fig. 7 in §5.1 shows that the differences from the case $\beta \rightarrow \infty$ are modest.

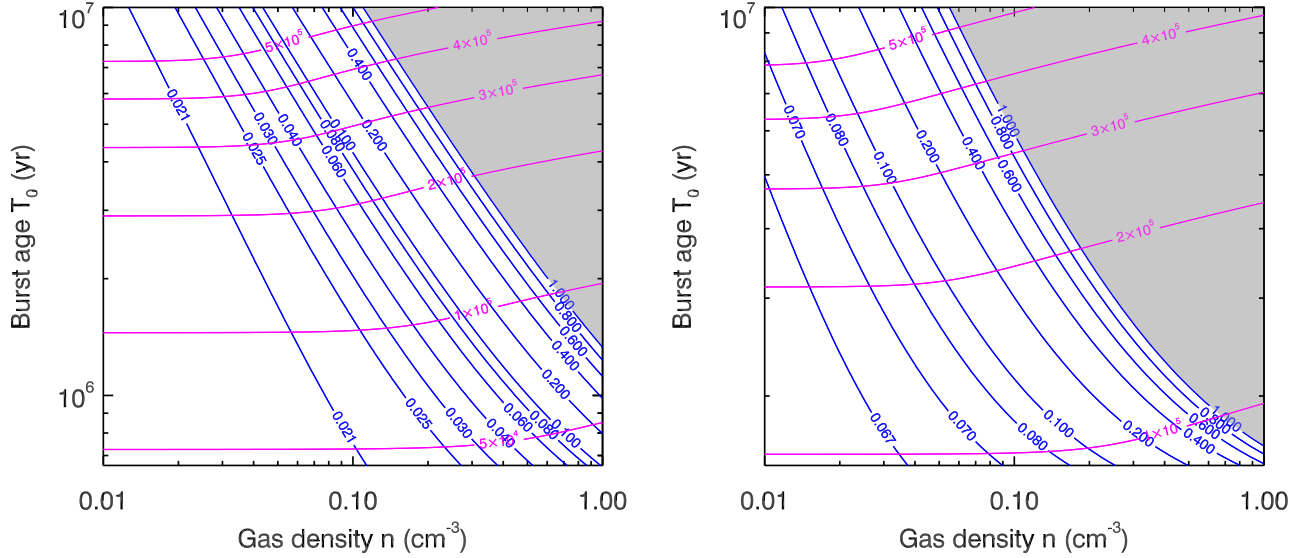


FIG. 10.— The required Eddington fraction as a function of burst age T_o and Stream gas density n_H . (Left) For $D = 55$ kpc and $\beta = 3$. (Right) For $D = 100$ kpc and $\beta = 6$. Compare with Fig. 7.

We mention briefly one further important point. The gas recombination/cooling times can obscure any natural variations in the source ionising luminosity. As discussed in the text, the Stream H α emission *must* arise from a fading source, but the fading time of the H α emission is limited by the gas recombination time, which imposes a transfer function on the luminosity variations. The source variation timescale τ_s could in principle be shorter, and the luminosity variations even more dramatic, than what we infer. In reality, the transfer function will be even more complex than what is implied by the simple model used here, since the real Stream gas has distributions of gas density and column density. In general, when comparing numerical models of AGN variability with the Stream emission (e.g. Novak et al 2011), the modelled data stream must be temporally convolved with a function whose bandwidth will depend on the gas density.

B. THE IMPLAUSIBILITY OF A STARBURST ORIGIN OF THE FLARE

Equation (3) provides a minimum estimate for the ionising photon luminosity needed to explain the Stream H α emission of $N_i \sim \text{a few} \times 10^{53} \text{ phot s}^{-1}$ — this assumes no fading of the emission and no significant absorption of the ionising photon flux. What starburst parameters does this imply?

Maloney (1999) quotes a ratio of ionising photon luminosity to star formation rate of

$$N_i / \dot{M}_* \sim 10^{53} \text{ phot s}^{-1} M_\odot^{-1} \text{ yr} \quad (\text{B1})$$

with substantial caveats on starburst age, upper and lower mass cutoffs, etc. This number agrees very well with the properties of the massive young star clusters formed in the Galactic Centre over the past several Myr: the Quintuplet, the Arches, and the Nuclear Cluster, which have total stellar masses $\sim 10^4 M_\odot$, ages in the range 1–7 Myr, and $N_i \sim 10^{51} \text{ phot s}^{-1}$ (Figer, McLean, & Morris 1999). Even for burst timescales as short as 1 Myr, the resulting star formation rates $\dot{M}_* \sim 0.01 M_\odot \text{ yr}^{-1}$, giving ionising photon luminosities per unit SFR in agreement with (B1). We can also use these observations to estimate the ionising photon flux per unit mass of stars formed: this is

$$N_i / M_* \sim 10^{47} \text{ phot s}^{-1} M_\odot^{-1}. \quad (\text{B2})$$

Powering the Stream emission at the minimal levels of eq. (3) thus requires a SFR of

$$\dot{M}_* \sim 1.4 - 4.7 M_\odot \text{ yr}^{-1} \quad (\text{B3})$$

and a total mass of stars formed of

$$M_* \sim (1.4 - 4.7) \times 10^6 M_\odot \quad (\text{B4})$$

The requirement of eq. (B3) exceeds by \sim two orders of magnitude all estimates of the SFR in the Galactic Centre within the last 1–100 Myr (e.g. Pfuhl et al 2011, their Fig. 14, and many references therein; see also above). A similar problem arises with the mass of stars in the Galactic Centre as a function of age (Pfuhl et al 2011). This number for the SFR is likely to be a substantial underestimate, since we have neglected extinction in the vicinity of the star-forming regions: for the three young Galactic Centre clusters discussed above, a large fraction of the emitted ionising photons are absorbed locally.

In fact, the situation is even worse than this: any such nuclear starburst would have to have declined in luminosity by ~ 2 orders of magnitude from the required peak luminosity to the present epoch, indicating that ~ 5 or more e -folding times have elapsed. For plausible minimum starburst timescales ($\tau_s \sim 2 - 3$ Myr), this makes the burst epoch too early to match the age of the *Fermi* bubbles. Except for implausibly small Stream densities ($n_H \sim 0.01 \text{ cm}^{-3}$), this also indicates that $\beta \lesssim 1$, and even though this will delay the decline of $\text{H}\alpha$ surface brightness compared to the case where the flare shuts off in a time $\tau_s \ll \tau_{\text{rec}}$ (see Appendix A), it also introduces a fine-tuning problem: unless we are catching the Stream emission at a time very close to τ_c as given by eq. (A21), the observed $\mu_{\text{H}\alpha}$ will be substantially less than the peak value, indicating that the peak SFR and the mass of stars formed in the burst would need to be even larger than the estimates of eqs. (B3) and (B4). Hence starburst models for the Stream $\text{H}\alpha$ emission are simply not viable: *the required star formation rates greatly exceed anything seen in the star formation history of the Galactic Centre.*

C. SPECTRAL ENERGY DISTRIBUTION OF AN ACCRETION DISK

Our model for the accretion disk comprises a ‘cool’ big blue bump and a ‘hot’ power law component. We define the specific photon luminosity for the two-component spectrum by

$$N_\bullet = k_1 (E/E_1)^{-2/3} e^{-E/E_1} + k_2 (E/E_2)^{-\alpha} e^{-E/E_2} \mathcal{H}(E - E_1) \quad \text{phot s}^{-1} \text{ eV}^{-1}, \quad (\text{C1})$$

where $\mathcal{H}[E - E_1] = 1$ if $E > E_1$ and $\mathcal{H}[E - E_1] = 0$ otherwise. Then the *total* AGN luminosity is given by

$$\begin{aligned} L_\bullet &= \int_0^\infty E N_\bullet dE \\ &= k_1 E_1^2 \int_0^\infty \epsilon^{1/3} e^{-\epsilon} d\epsilon + k_2 E_2^2 \int_{w_2}^\infty \mu^{1-\alpha} e^{-\mu} d\mu \\ &= L_0 + L_2 \end{aligned} \quad (\text{C2})$$

where $\epsilon \equiv E/E_1$, $\mu \equiv E/E_2$, and $w_2 \equiv E_1/E_2$.

Taking the hydrogen ionisation potential, $I_H = 13.59844 \text{ eV}$, and $w_1 = I_H/E_1$, the AGN ionising luminosity is found by integrating from the Lyman limit to infinity,

$$\begin{aligned} L_{\bullet,i} &= \int_{w_1}^\infty E N_\bullet dE \\ &= k_1 E_1^2 \int_{w_1}^\infty \epsilon^{1/3} e^{-\epsilon} d\epsilon + k_2 E_2^2 \int_{w_2}^\infty \mu^{1-\alpha} e^{-\mu} d\mu \\ &= L_1 + L_2 \end{aligned} \quad (\text{C3})$$

where the limit for the second integral remains the same since $w_2 > w_1$.

The big blue bump *total* contribution is

$$L_0 = k_1 E_1^2 \Gamma\left(\frac{4}{3}\right) \quad (\text{C4})$$

where $\Gamma(a)$ is the complete gamma function. The big blue bump ionising contribution is

$$L_1 = k_1 E_1^2 \Gamma\left(\frac{4}{3}, w_1\right) \quad (\text{C5})$$

and, finally, the third integral (the power-law X-ray + gamma-ray contribution) is

$$L_2 = k_2 E_2^2 \Gamma(2 - \alpha, w_2) \quad (\text{C6})$$

where we use the incomplete gamma function, $\Gamma(a, b)$, and α must be less than 2. Here we adopt a photon spectral index of $\alpha = 1.9$.

If we define $\eta \equiv L_1/L_2$, so that $L_2 = L_{\bullet,i}/(1 + \eta)$ and $L_1 = \eta L_2$, then we can write k_1 and k_2 as

$$k_1 = L_{\bullet,i} E_1^{-2} \left[\frac{\eta}{\Gamma(4/3, w_1)(1 + \eta)} \right], \quad (\text{C7})$$

$$k_2 = L_{\bullet,i} E_2^{-2} \left[\frac{1}{\Gamma(2-\alpha, w_2)(1+\eta)} \right]. \quad (C8)$$

The scaling coefficient ratio k_1/k_2 is independent of $L_{\bullet,i}$ such that

$$\frac{k_1}{k_2} = \eta \left[\frac{E_2^2}{E_1^2} \right] \frac{\Gamma(2-\alpha, w_2)}{\Gamma(4/3, w_1)}. \quad (C9)$$

Once the AGN luminosity L_{\bullet} and UV to X- γ ratio (η) are specified, the normalisation constants k_1 and k_2 follow immediately (see §2).

REFERENCES

- Acosta-Pulido JA et al 1990, ApJ, 365, 119
 Alexander DM & Hickox RC 2012, ApJ, 56, 93
 Alexander T et al 2000, ApJ, 536, 710
 Antonucci R 1993, ARAA, 31, 473
 Baker DJ & Romick GJ 1976, Appl. Opt., 15, 1666
 Barger K et al 2013, ApJ, 771, 132
 Begelman MC & Bland-Hawthorn J 1998, Nat, 385, 22
 Besla G et al 2012, MNRAS, 421, 2109
 Blandford RD & Begelman M 1999, MNRAS, 303, L1
 Bland-Hawthorn J & Cohen M 2003, ApJ, 582, 246
 Bland-Hawthorn J & Maloney PR 1999, ApJ, 522, L81
 Bland-Hawthorn J & Maloney PR 2002, ASPC, 254, 267
 Bland-Hawthorn J, Sutherland RS, Agertz O & Moore B 2007, ApJ, 670, L109
 Carretti E et al 2012, Nat, 493, 66
 Cecil GN 1988, ApJ, 329, 38
 Dermer CD et al 1997, ApJ, 484, L121
 Dobler G et al 2010, ApJ, 717, 825
 Dopita MA, Sutherland RS et al 2013, ApJS, 208, 10
 Duric N et al 1983, ApJ, 273, L11
 Figer DF, McLean IS & Morris M 1999, ApJ, 514, 202
 Finkbeiner DP 2004, astro-ph/0409027
 Fox A et al 2010, ApJ, 718, 1046
 Fox A et al 2013, ApJ, 772, 110
 Freitag M et al 2006, ApJ, 649, 91
 Genzel R et al 2003, Nat, 425, 934
 Genzel R, Eisenhauer F & Gillessen S 2010, Rev. Mod. Phys., 82, 3121
 Gillessen S et al 2013, ApJ, 763, 78
 Guo F & Mathews WG 2012, ApJ, 756, 181
 Hawley JF & Balbus SA 2002, ApJ, 573, 738
 Ho P 2008, ARAA, 46, 475
 Hopkins P & Hernquist LE 2006, ApJS, 166, 1
 Jin S & Lynden-Bell D 2008, MNRAS, 383, 1686
 Jolley EJD & Kuncic Z 2008, ApJ, 676, 351
 Kaffle P et al 2012, ApJ, 761, 98
 Kalberla PM et al, A&A, 440, 775
 Keel WC et al 2006, AJ, 132, 2233
 Keeney BA et al 2006, ApJ, 645, 951
 Kormendy J & Ho PT 2013, ARAA, in press (astro-ph/1304.7762)
 Koyama K et al 1996, PASJ, 48, 249
 Kreimeyer K & Veilleux S 2013, ApJ, 772, L11
 Krolik JH & Begelman 1986, ApJ, 308, L55
 Lehner N & Howk JC 2010, ApJ, 709, L138
 Lu JR et al 2013, ApJ, 764, 155
 Lutz D et al 2000, ApJ, 536, 697
 Madau P 1988, ApJ, 327, 116
 Madsen G et al 2001, ApJ, 560, L135
 Madsen G 2012, EAS Publ. Series, 56, 281
 Madsen G et al 2013, ApJ, in prep.
 Maloney PR 1999, A&SS, 266, 207
 Mathewson DS, Cleary JD & Murray MN 1974, ApJ, 190, 291
 Mathewson DS & Ford VL 1984, in Structure & Evolution of the Magellanic Clouds, IAU Symp., 108, 125
 McClure-Griffiths N et al 2013, ApJ770, L4
 Meyer L, Ghez A et al 2012, Sci, 338, 84
 Moore B & Davis M 1994, MNRAS, 270, 209
 Mortlock D et al 2011, Nat, 474, 616
 Mulchaey J, Wilson AS & Tsvetanov Z 1996, ApJ, 467, 197
 Nichols M et al 2011, ApJ, 742, 110
 Nidever DL, Majewski SR & Butler WB 2008, ApJ, 679, 432
 Nigra L et al 2012, ApJ, 760, 48
 Novak G, Ostriker J & Ciotti L, 2011, ApJ, 737, 26
 Novak G, Ostriker J & Ciotti L, 2012, MNRAS, 427, 2734
 Paumard T et al 2006, ApJ, 643, 1011
 Pfuhl O et al 2011, ApJ, 741, 108
 Ponti G et al 2010, ApJ, 714, 732
 Ponti G et al 2013, Astro. Space Sci. Proc., 34, 331
 Proga D, Stone JM & Kallman TR 2000, ApJ, 543, 686
 Proga D & Kallman TR 2004, ApJ, 616, 688
 Putman ME et al 1998, Nat, 394, 752
 Putman ME et al 2003, ApJ, 597, 948
 Putman ME, Peek JEG & Joungh MR, 2012, ARAA, 50, 491
 Requena-Torres MA et al 2012, A&A, 542, L21
 Reynolds RJ et al 1998, PASA, 15, 14
 Richter P et al 2013, ApJ, 772, 111
 Robitaille TP & Whitney BA 2010, ApJ, 710, L11
 Rupke D & Veilleux S 2013, ApJ, 768, 75
 Sharp RG & Bland-Hawthorn J 2010, ApJ, 711, 818
 Sim SA et al 2010, MNRAS, 408, 1396
 Slavin JD, McKee CF & Hollenbach DJ 2000, ApJ, 541, 218
 Sokolowski J et al 1991, ApJ, 375, 583
 Spitzer L 1978, Physical Processes in the Interstellar Medium (Wiley: New York)
 Stanimirović, S et al 2008, ApJ, 680, 276
 Su M & Finkbeiner DP 2012, ApJ, 753, 51
 Su M, Slayter TR & Finkbeiner DP 2010, ApJ, 724, 1044
 Sunyaev RA et al 1993, ApJ, 407, 606
 Tadhunter C & Tsvetanov Z 1989, Nat, 341, 422
 Tsvetanov Z et al 1996, ApJ, 458, 172
 Wardle M & Yusef-Zadeh F 2008, ApJ, 683, L37
 Wehrle & Morris 1987, ApJ, 313, L43
 Wehrle & Morris 1988, AJ, 95, 1689
 Weiner BJ, Vogel SN & Williams TB 2002, ASPC, 254, 256
 Weiner BJ & Williams TB 1996, AJ, 111, 1156
 Weymann RJ et al 2001, ApJ, 561, 559
 Wild V et al 2013, A&A, in press
 Yusef-Zadeh F et al 2012, ApJ, 758, L11
 Zubovas K, King AR & Nayakshin S 2011, MNRAS, 415, L21